


Summer 2018

A System For Conducting Laser-Induced Fluorescence Measurements On Gas Mixtures Exposed To Alpha Radiation

Patrick Ables
University of Southern Mississippi

Follow this and additional works at: https://aquila.usm.edu/masters_theses

 Part of the [Atomic, Molecular and Optical Physics Commons](#), [Environmental Chemistry Commons](#), [Optics Commons](#), and the [Radiochemistry Commons](#)

Recommended Citation

Ables, Patrick, "A System For Conducting Laser-Induced Fluorescence Measurements On Gas Mixtures Exposed To Alpha Radiation" (2018). *Master's Theses*. 371.
https://aquila.usm.edu/masters_theses/371

This Masters Thesis is brought to you for free and open access by The Aquila Digital Community. It has been accepted for inclusion in Master's Theses by an authorized administrator of The Aquila Digital Community. For more information, please contact Joshua.Cromwell@usm.edu.

A SYSTEM FOR CONDUCTING LASER-INDUCED FLUORESCENCE
MEASUREMENTS ON GAS MIXTURES EXPOSED TO ALPHA RADIATION

by

Patrick Ross Ables

A Thesis

Submitted to the Graduate School,
the College of Science and Technology
and the Department of Physics and Astronomy
at The University of Southern Mississippi
in Partial Fulfillment of the Requirements
for the Degree of Master of Science

Approved by:

Dr. Christopher B. Winstead, Committee Chair
Dr. Khin Maung Maung, Member
Dr. Jeremy Scott, Member
Dr. Michael D. Vera, Member

Dr. Christopher B.
Winstead
Committee Chair

Dr. Khin Maung Maung
Department Chair

Dr. Karen S. Coats
Dean of the Graduate School

August 2018

COPYRIGHT BY

Patrick Ross Ables

2018

Published by the Graduate School



THE UNIVERSITY OF
SOUTHERN
MISSISSIPPI.

ABSTRACT

This paper documents modifications to an existing vacuum system to allow laser-induced fluorescence spectroscopy measurements within simulated atmospheres under a variety of conditions. This added capability will expand the laboratory's ability to experimentally validate a computational model that calculates the effects of radiation within the atmosphere. The computational model could reveal radiation-induced chemical products that can be used to develop an alternative detection method that can be implemented from a safe distance. The selection of molecules for experimental validation has been limited to those which can be detected utilizing cavity ringdown spectroscopy. The current model indicates nitric oxide and ozone to be the primary reactants that dictate production rates and concentrations for many of the resulting chemical products. Because strong absorption cross sections for nitric oxide are too deep in the ultraviolet to effectively use the cavity ringdown method, laser-induced fluorescence spectroscopy was seen as a viable alternative. Using a certified mix of NO₂ and a second mix of NO, the system is validated by stepping a dye laser through wavelengths from 225.9 nm to 227.1 nm. The data collected was used to produce an excitation spectrum to compare with a simulated spectrum. These mixes were diluted with an ultra-high purity grade of N₂ so that an experimental detection limit could be approximated. The excitation spectrum produced is in excellent agreement with that of the simulated spectrum and an experimental approximation of the detection limit for NO was found to be 3 ± 2 parts-per-billion in a background of N₂.

ACKNOWLEDGMENTS

I would like to thank Dr. Chris Winstead for his confidence and for providing me with the opportunity to be a member of his research group. I appreciate his mentorship and guidance along the way. The experience has helped me to become a better scientist. Thank you to the rest of my committee members, Dr. Khin Maung, Dr. Michael Vera, and Dr. Jeremy Scott, for their advice and time helping to refine this document. I want to thank my lab partners Tyler Reese and Sidney Gautrau for their fraternity and for providing an excellent research environment. Tyler was always there to answer questions about the research project, to lend a hand with small jobs, and to give his opinion on various system modifications. Sidney and I worked together to write the software that runs the lab's experimental system and collaborated on many of modifications outlined in this thesis.

DEDICATION

I would like to dedicate this thesis to my parents, Ross and Pam Ables, and to my grandmother, Lucille Ables. Without their years of encouragement and support, I would not be where I am today.

TABLE OF CONTENTS

ABSTRACT ii

ACKNOWLEDGMENTS iii

DEDICATION iv

LIST OF TABLES vii

LIST OF ILLUSTRATIONS viii

LIST OF ABBREVIATIONS x

CHAPTER I – INTRODUCTION 1

CHAPTER II – A SHORT DESCRIPTION OF RADIOACTIVE DECAY 3

CHAPTER III – LASER-INDUCED FLUORESCENCE 9

CHAPTER IV – EXISTING SYSTEMS UTILIZED 15

 Vacuum System 15

 Physical Description & Port Usage..... 16

 Pumping Systems..... 21

 Measurement Capability 22

 Control System..... 22

 Laser System..... 23

 Data Acquisition System..... 25

CHAPTER V – SYSTEM MODIFICATIONS 26

 Vacuum System Modifications..... 26

New Source Box	27
Extension Linkage	28
Adjustable Platform Voltage.....	30
Control System Modifications	33
Laser-Induced Fluorescence System.....	33
Laser System Modifications	33
Sum Frequency Mixing.....	36
Dark Room.....	40
DAQ System	41
CHAPTER VI – SOFTWARE DEVELOPMENT	43
Laboratory Network.....	44
Control Software.....	46
“Vacuum System Control.vi”	47
“Ringdown Time.vi”	54
“Dye Laser Control.vi”	59
CHAPTER VII – SYSTEM VERIFICATION AND RESULTS	61
CHAPTER VIII – CONCLUSIONS AND FUTURE WORK.....	73
APPENDIX A – Permission Emails	76
APPENDIX B	80
REFERENCES	81

LIST OF TABLES

Table 1 Penetration Depth Comparison for Representative Radiation Sources	8
Table 2 Wavelength vs. Motor Position	39

LIST OF ILLUSTRATIONS

Figure 1. Uranium-238 Decay Chain.....	8
Figure 2. Internal transitions between molecular states.....	10
Figure 3. Energy state diagram.....	14
Figure 4. Initial configuration of existing vacuum chamber.....	17
Figure 5. Vacuum chamber and gas introduction manifold.....	18
Figure 6. Custom 8” flanges for CRDS.....	19
Figure 7. Original source holder and shield.....	20
Figure 8. Polonium-210 alpha source.....	21
Figure 9. Electronics housing with cRIO.....	23
Figure 10. Nd:YAG and Dye lasers.....	24
Figure 11. Existing data acquisition system.....	25
Figure 12. New radiation source box.....	28
Figure 13. Extension linkage design for source box.....	29
Figure 14. Extension linkage installed.....	30
Figure 15. Electrically insulated stainless support.....	31
Figure 16. New configuration of existing vacuum chamber.....	32
Figure 17. Modified dye and Nd:YAG lasers.....	35
Figure 18. Polarization Rotation Diagram.....	36
Figure 19. FCU: BBO, compensator, and dichroic.....	38
Figure 20. FCU: Wavelength separator.....	39
Figure 21. Laser system path.....	40
Figure 22. Dark room.....	41

Figure 23. Data acquisition system.....	42
Figure 24. Laboratory network diagram.....	45
Figure 25. “Vacuum System Control.vi” Controls tab.....	51
Figure 26. “Vacuum System Control.vi” Automated Task tab.....	52
Figure 27. “Vacuum System Control.vi” Maintenance tab.....	53
Figure 28. “Ringdown Time.vi” Ringdown tab.....	56
Figure 29. “Ringdown Time.vi” LIF tab.....	57
Figure 30. “Ringdown Time.vi” scope tab.....	59
Figure 31. “Dye Laser Control” Sirah Control tab.....	60
Figure 32. LIFBASE program and example spectrum.....	62
Figure 33. Spectrum from initial verification run with NO ₂	64
Figure 34. NO ₂ Hysteresis and reproducibility check.....	65
Figure 35. Fluorescence from NO ₂ mix with decreasing concentration.....	67
Figure 36. Raw fluorescence signal with decreasing concentration.....	69
Figure 37. NO fluorescence response with decreasing concentration.....	70
Figure 38. NO fluorescence response from lowest concentrations.....	71
Figure 39. Integrated NO fluorescence response.....	72

LIST OF ABBREVIATIONS

amu	atomic mass unit
BBO	beta Barium Borate
CRDS	cavity ring down spectroscopy
cRIO	compact reconfigurable input/output device
HG	harmonic generator
LabVIEW	laboratory Virtual Instrument Engineering Workbench
LIF	laser-induced fluorescence
Nd:YAG	Neodymium-doped Yttrium Aluminum Garnet
NI	National Instruments
NI-PSP	NI Publisher-Subscriber Protocol
PMT	photomultiplier tube
ppb	parts per billion
ppm	parts per million
SFM	sum frequency mixing
SVE	LabVIEW's Shared Variable Engine
TTL	transistor-transistor logic
UGA	Universal Gas Analyzer
UHP	ultra high purity
UV	ultraviolet
VI	LabVIEW's Virtual Instrument

CHAPTER I – INTRODUCTION

The current project is funded by a DTRA grant and has the goal of creating a computational model for calculating the effects of radiation within the atmosphere under a variety of conditions. The usual method of detecting radiation involves sending a person into the suspected area of radioactivity with a hand-held device putting the user at risk of being exposed to potentially high levels of radiation. Once complete, the computational model could uncover unique chemical products which may lead to a safer, long distance detection method. Experimental work is necessary to validate the model. Previous work performed under this grant has successfully measured the radiation-induced production rates of ozone (O_3) using a spectroscopy method known as cavity ring down spectroscopy (CRDS).

Another molecule of experimental interest to the project is nitric oxide (NO). CRDS relies on the availability of highly reflective mirrors to create an optical cavity to effectively extend the path length of a tuned laser beam. A time constant associated with the exponential decay in intensity is calculated with and without a particular absorber present. The difference between the two decay constants is used to determine the specific molecular number density accounting for cavity related losses. With respect to lasing wavelengths, the detection limit of this method in the deep UV is relatively high due to poor mirror coatings. A strong absorption spectrum for NO is unfortunately in this deep UV range making CRDS unviable. A spectroscopy method known as laser-induced fluorescence (LIF) has the necessary sensitivity for probing low molar fractions of NO by measuring its fluorescence signal from a location perpendicular to the exciting laser's path. Modifying the experimental system to utilize LIF will expand the lab's capacity to

detect radiation-induced chemical products. It was beneficial to modify the vacuum system to accommodate LIF experiments without losing CRDS capabilities. This paper will document these system modifications, demonstrate the LIF system is capable of measuring NO in a background of N₂ and experimentally show the detection limit is well below the proposed concentration induced by radiation in the atmosphere.

This thesis covers a short description of radioactive decay, an explanation of laser-induced fluorescence, a description of the existing systems, modifications made to the vacuum system to accommodate the geometry necessary for LIF measurements and improve the shielding of the radioactive sources, alterations to the optical systems to allow sum frequency mixing, changes to the data acquisition system that increase the temporal resolution of measurements, a description of each software program used to run the system, and a section documenting the results of fluorescence measurements made to verify system sensitivity. It is meant to chronicle the evolution of each experimental system in the laboratory as a reference for future students.

Verification of the LIF system is done by performing fluorescence measurements first on a certified mix of 5 ppm NO₂ in a balance of N₂, then on a certified mix of 100 ppb NO gas in N₂. Both mixes were diluted with ultra-high-purity (UHP) N₂ to effectively reduce the concentration for running additional fluorescence measurements to estimate a minimum detection limit. The excitation spectrum collected from both mixes agree well with a simulated NO spectrum produced by a freeware program called LIFBASE. The exciting beam is also shown to have sufficient linewidth for detecting NO within the A²Σ⁺ to X²Π schemes with an experimentally determined detection limit around 3 ± 2 ppb in a background of N₂.

CHAPTER II – A SHORT DESCRIPTION OF RADIOACTIVE DECAY

Radioactive decay is the process in which a particle or photon is spontaneously emitted from an unstable atomic nucleus, termed radionuclide, effectively decaying into a lighter, and in some cases more stable, atom. The radioactive decay process continues with the resulting atom if a stable nucleus is not produced. Series radionuclides can take many steps before producing a stable nucleus. The decay chain is unique to each series and all the products within the chain are radioactive except the final.

Each species of radionuclide has a unique decay rate. Some decay in seconds while others take millions, even billions of years. Since the decay process happens spontaneously, the precise time a single radionuclide will decay cannot be predicted; however, after a period of time statistics show a collection of a single species will decay with an average rate that depends on the initial number of atoms. The standard half-life used for expressing decay rates refers to the time it takes for one half the initial number of a particular species of radionuclides present in a sample to decay. A mathematical derivation of this concept is as follows:

$$-\frac{dN}{dt} = \lambda N \quad (2.1)$$

The change in the number of radioactive atoms, N , with respect to time, t , is equal to some decay rate constant, λ , multiplied by the number of radioactive atoms.

Moving N to the LHS, integrating and solving for N , this expression becomes:

$$N = N_0 e^{-\lambda t} \quad (2.2)$$

The number of radioactive atoms, N , after some period of time, t , is equal to the initial number of radioactive atoms, N_0 , multiplied by the exponential factor, e , to the power $-\lambda$, the decay rate constant, multiplied by said time period.

Dividing each side of Eq. 2.2 by N_0 , then setting it equal to one half, the expression for a half-life can be found.

$$\begin{aligned} \frac{1}{2} &= \frac{N}{N_0} = \exp(-\lambda t_{1/2}) \\ t_{1/2} &= \frac{\ln 2}{\lambda} \end{aligned} \quad (2.3)$$

The half-life time, $t_{1/2}$, is equal to the natural log of two divided by the decay rate constant, λ .¹²

The half-life also indicates when the radiation intensity resulting from a radioactive sample reduces by a factor of one half. To calculate the current radioactivity of a sample, its half-life, the initial intensity and the time elapsed since that initial intensity was measured are all that is required. Named in honor of Madam Curie's work, the Curie is the standard unit for expressing radioactivity and is equal to 3.7×10^{10} decays per second.

There are three main types of ionizing radiation: alpha particles, beta particles, and gamma rays. Alpha particles are identical to the nucleus of a stable ^4He atom,

¹ J. E. Turner, *Atoms, Radiation, and Radiation Protection*, 3rd completely rev. and enl. ed, Physics Textbook (Weinheim: Wiley-VCH, 2007), <http://nuclear.dababneh.com/Radiation-Undergrad/Atoms, Radiation, and Radiation Protection.pdf>.

² Dudley G. Miller, *Radioactivity and Radiation Detection* (Gordon and Breach Science Publishers, 1972).

composed of two protons and two neutrons. They are emitted from the nucleus of certain radionuclides during the decay process which reduces its mass by four amu leaving it with a charge of $Z-2$, where Z is the number of protons in the nucleus.³ Most producers of this type of radiation are heavier elements but a few alpha emitters under 83 amu exist.⁴ Because of their large mass, alpha particles resist the usual scattering processes affecting other forms of ionizing radiation and deposit all of their energy through particle collisions over a distance of only a few centimeters when attenuated by air at standard atmospheric pressure. Alpha particles emitted by the same species carry approximately the same energy.⁵ While dangerous if ingested or inhaled, alpha emitters pose no danger to life in general, lacking the energy to penetrate the outermost epidermal layer of dead skin.⁶

Beta particles are essentially electrons. When a neutron in the nucleus of a radionuclide decays into a proton and electron, the proton remains a part of the nucleus while the electron is ejected along with an anti-neutrino. Despite their relatively small mass, these tiny particles carry away a significant amount of kinetic energy because of the high velocities with which they are ejected. This process reduces the total nuclear mass by that of the electron and anti-neutrino plus the mass equivalent of the binding

³ Aubrey D. Mcfadyen, "Samuel C. Lind," *Chemical & Engineering News* 25, no. 23 (June 9, 1947): 1664, <https://doi.org/10.1021/cen-v025n023.p1664>.

⁴ Turner, *Atoms, Radiation, and Radiation Protection*.

⁵ Mcfadyen, "Samuel C. Lind."

⁶ Doran M. Christensen, Carol J. Iddins, and Stephen L. Sugarman, "Ionizing Radiation Injuries and Illnesses," *Emergency Medicine Clinics of North America* 32, no. 1 (February 2014): 245–65, <https://doi.org/10.1016/j.emc.2013.10.002>.

energy between the dissociated proton and electron and leaves the newly transformed nucleus with a charge of $Z+1$. Contrary to that of an alpha particle, the energy of a beta particle can be within a wide range of values bound by a fixed upper limit.⁷ Like alphas, betas lose energy through particle collisions but are easily scattered from their original paths because of their relatively small mass. As a result, these particles deposit all of their ionizing energy within a distance of several meters through dry air.⁸

Gamma rays are high energy photons typically produced by the nuclei of unstable atoms to remove excess vibrational energy after an alpha or beta emission leaves them in an excited state. Since photons have no mass or charge, a gamma emission does not alter the nucleic charge or mass. As with alpha particles, gamma rays produced by the same radionuclidic species carry almost the same energy. This energy is dissipated through the air within a distance on the order of a couple hundred meters due to Compton scattering, photo ionization (photoelectric effect), and/or particle/antiparticle pair production.⁹

With a half-life of 138.4 days, ^{210}Po supplies the ionizing alpha radiation in the experimental work proposed in this thesis. It is the last radioactive link in the ^{238}U decay chain stabilizing as ^{206}Pb after an alpha emission. This particular source was chosen by Reese for his work on a similar project after calculating the range and energy output for each source type. The results of those calculations are shown in Table 1 with his permission and show the expected range for a ^{210}Po , ^{90}Sr , and ^{60}Co source assuming

⁷ Turner, *Atoms, Radiation, and Radiation Protection*.

⁸ William James Price, *Nuclear Radiation Detection* (McGraw-Hill, 1964); Michael F. L'Annunziata, *Radioactivity: Introduction and History* (Elsevier, 2007).

⁹ Price, *Nuclear Radiation Detection*.

attenuation by dry air near sea level.¹⁰ Because the literature source Reese used to determine stopping power lists discrete energy values, the values nearest to those in column 3 were used to approximate the expected range. Those nearest energy values are listed in column 4 for reference.

Figure 1 shows the ^{238}U decay chain depicting the decay path, emission type, decay product and respective half-life for each. While not shown in the figure, most decay products emit gamma rays in addition to the alpha or beta particle ejected during the decay process but ^{210}Po does not. The majority of rays produced from this process carry less than 500 keV of energy; however, ^{231}Bi radiates these high energy photons in the MeV range.¹¹

¹⁰ Tyler Reese, “A System for Measuring Radiation Induced Chemical Products in Atmospheric Gases Using Optical Detection Methods” (The University of Southern Mississippi, 2010).

¹¹ “Palos Verdes Radon,” United States Geological Survey, accessed December 24, 2017, <https://pubs.usgs.gov/of/2004/1050/PalosVerdesRn.htm#uranium.htm>.

Table 1 Penetration Depth Comparison for Representative Radiation Sources

Table by Tyler Reese. ¹² Reproduced with permission.

Radiation Type	Source	Energy Values of Emitted Radiation (MeV)	Nearest Energy Value with Mass Attenuation Provided (MeV)	Expected Range (m)
Alpha	²¹⁰ Po	5.3	5.5	0.042
Beta	⁹⁰ Sr	0.546, 2.28	0.55, 2.5	1.89, 11.4
Gamma	⁶⁰ Co	1.17, 1.33	1.25	146.2*

*Gamma range corresponds to distance at which the intensity is expected to be reduced by a factor of 1/e

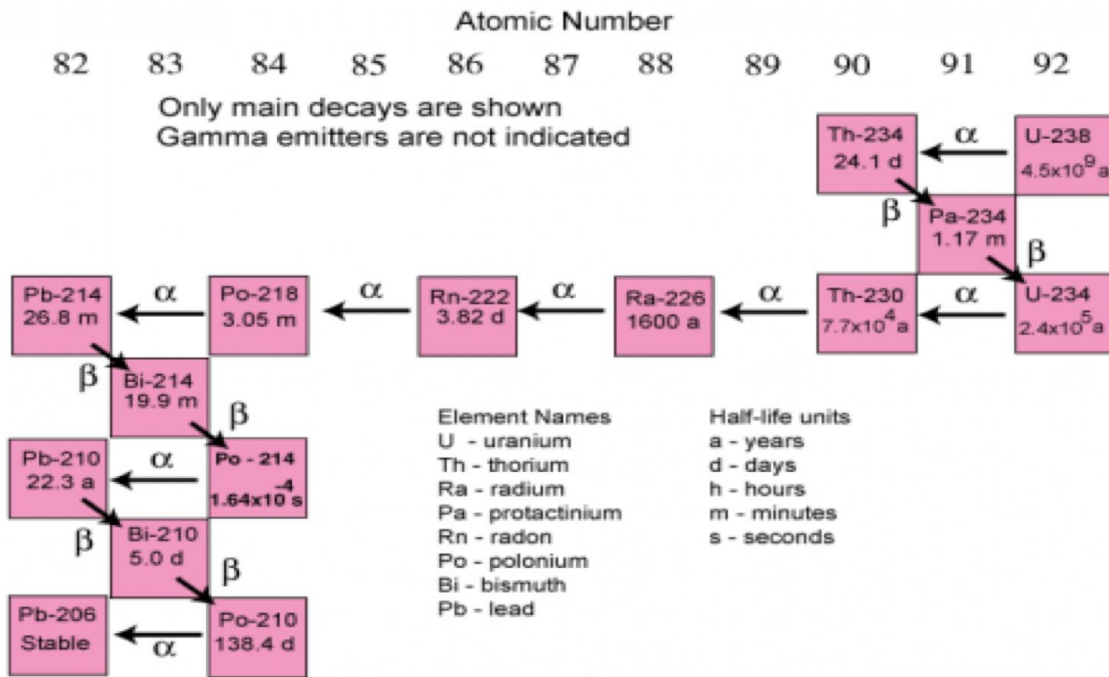


Figure 1. Uranium-238 Decay Chain

Decay chain for U²³⁸. The arrow and symbol between each box indicates the decay path and emission type while each box identifies the decay product and its respective half-life.¹³

¹² Reese, "A System for Measuring Radiation Induced Chemical Products in Atmospheric Gases Using Optical Detection Methods."

¹³ "Palos Verdes Radon."

CHAPTER III – LASER-INDUCED FLUORESCENCE

Incandescence refers to the process by which a hot body emits radiation merely from its high temperature. Any other form of photonic radiation within the visual spectrum is called luminescence. Photoluminescence occurs when a photon from an external light source supplies energy to a particle in a process known as absorption, which excites the particle to a higher energy state causing it to radiate away the excess energy by an emission of a new photon. The exciting light absorbed can be from the infrared, visible or ultraviolet part of the electromagnetic spectrum. Taking advantage of this property allows scientists explore the nature of various molecular species by means of fluorimetric analysis.¹⁴

Most molecules are in the lowest vibrational level of the electronic ground state when at room temperature. In addition to particle collisions, a molecule can be raised to a higher energy state by interacting with individual photons of light as mentioned before. The resulting excitation places the molecule into a rotational state within one of the electronic vibrational bands determined by the energy supplied from the absorbed photon. Because light and the molecular states are quantized, the energy added to the system is discrete and results in a discrete number of absorption bands. If a molecule is excited to a higher vibrational band of an excited state, particle collisions quickly reduce its excess vibrational energy causing it to fall to one of the lower bands of the excited state. The lower vibrational levels associated with one electronic level tend to overlap with the

¹⁴ A.T.R. Williams, *An Introduction to Fluorescence Spectroscopy* (Perkin-Elmer, 1981),

<https://books.google.com/books?id=CVL-ewEACAAJ>.

higher ones from the next lowest energy level. The diagram in Figure 2 serves as a visual depiction of these overlapping states.¹⁵ Most excitations to electronic levels greater than the second quickly cause internal transitions to occur that reduce the molecule to the next lower electronic level in a high vibrational band of the same energy where particle collisions further reduce its energy to that of a lower vibration band. This process continues until the first electronic state is reached. From the first electronic level, the molecule can continue to reduce its energy and return to a vibrational band of the ground state by emitting a photon in a process known as fluorescence.

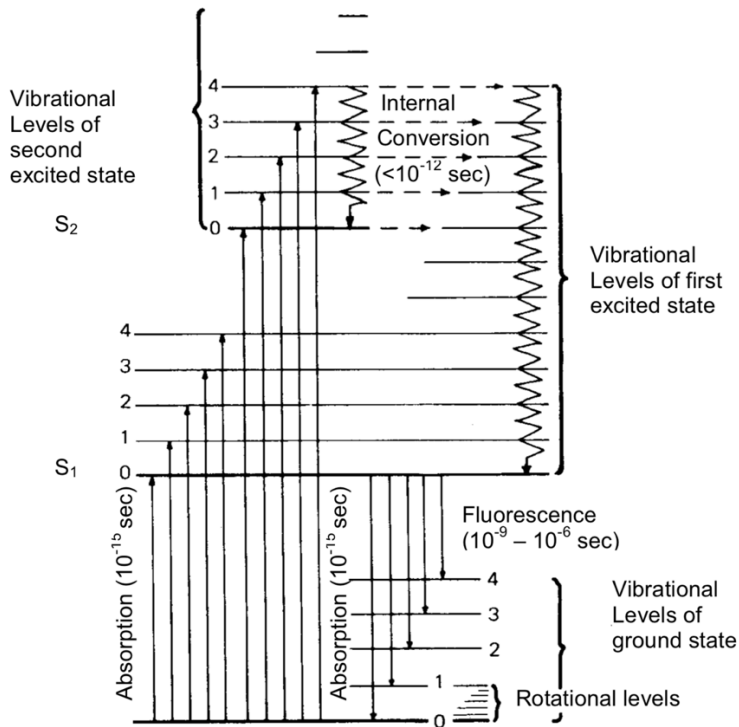


Figure 2. Internal transitions between molecular states

Diagram showing the overlapping molecular energy bands that allow internal transitions to occur after the molecule is excited.

© 2010-2018 PerkinElmer, Inc. All rights reserved. Printed with permission.

¹⁵ Williams.

Laser-induced fluorescence (LIF) spectroscopy, is a spectroscopic method that uses fluorescence to quantitatively measure or detect a particular molecular species within a sample. A laser is tuned to a frequency that corresponds to an absorption line of an atom or molecule of interest; after the individual atoms or molecules absorb one of these photons, they are excited to a higher electronic energy level which is followed by a spontaneous emission of light. The photons emitted from the sample are then detected by an instrument such as a photomultiplier or charge coupled device. LIF has played a major role in the study of the electronic spectra and structure of small molecules. The initial and excited state associated with a particular absorption line each have definite vibrational, rotational and fine structure quantum numbers offering this technique substantial selectivity beneficial to a wide array of spectroscopic and collision studies.¹⁶

There are a variety of LIF techniques that are not possible with non-laser spectroscopy, making it a highly versatile method for discovering new information about a system. For example, with a combination of plano-cylindrical lenses and a CCD, it is possible to record two and three-dimensional images of the fluorescence distribution.¹⁷ LIF has many advantages over other laser based spectroscopic methods. Since the fluorescence response of each molecular species results in a unique spectrum, the probing wavelength can be swept through a particular excitation spectrum not shared by other background gases. The selectivity this adds translates to a very high signal-to-noise ratio,

¹⁶ David R. Crosley, "Laser-Induced Fluorescence in Spectroscopy, Dynamics, and Diagnostics," *Journal of Chemical Education* 59, no. 6 (June 1982): 446, <https://doi.org/10.1021/ed059p446>.

¹⁷ Williams, *An Introduction to Fluorescence Spectroscopy*.

making LIF an ideal diagnostic tool to definitively identify a particular species within a sample gas. LIF has good sensitivity even over short path lengths providing an alternative spectroscopic approach to CRDS, especially in the UV spectral range where mirror coatings are too poor to work effectively.¹⁸

When measuring fluorescence, the cumulative signal from a collection of fluorescers is measured by a detector such as a photomultiplier, which typically uses a bandpass filter to help minimize contributions from the scattered laser light probe. Fluorescence happens isotropically, *i.e.* radially in every direction, which allows a detector to be placed at any location with a line-of-sight to the exciting beam path. The photomultiplier is usually placed perpendicular to this axis which helps to minimize the amount of scatter from the exciting light sent in the direction of the tube. Another common detection method utilizes a spectrometer with a diffraction grating to separate the signal before imaging it onto a charge coupled device (CCD). Segments of the CCD correspond to a particular wavelength enabling one to approximate the number density of each molecular state and help distinguish fluorescence from the scattered exciting wavelength.¹⁹ Traditional quantitative measurements require several measurements such as the solid angle between the detector and beam path and the volume of space in which the beam travels through the sample. These measurements introduce significant error to the quantitative calculation contributing to a high degree of uncertainty particularly for low number densities.

¹⁸ Williams.

¹⁹ Williams.

Two photon excitations expand the probing abilities of an experimental spectroscopy setup. These excitations occur when one photon photodissociates a molecule and a second photon of the same frequency excites one of the fragments. Photodissociation is a photo-chemical process that happens when an incident photon has enough energy to sever the bond between two atoms or secondary molecules. NO_2 is a good example of this process since a 226 nm photon will photodissociate it into a free oxygen and an NO molecule. In the two-photon excitation scheme, the NO fragment absorbs a second 226 nm photon, causing it to fluoresce and radiate away the extra energy to return to the electronic ground state. Figure 3 depicts this excitation and the spontaneous emission that follows for nitric oxide between its first electronic level and its ground state. Although the arrows indicate a specific direction, the excitation can occur from either direction, i.e. the direction of the arrows on the diagram can be reversed.

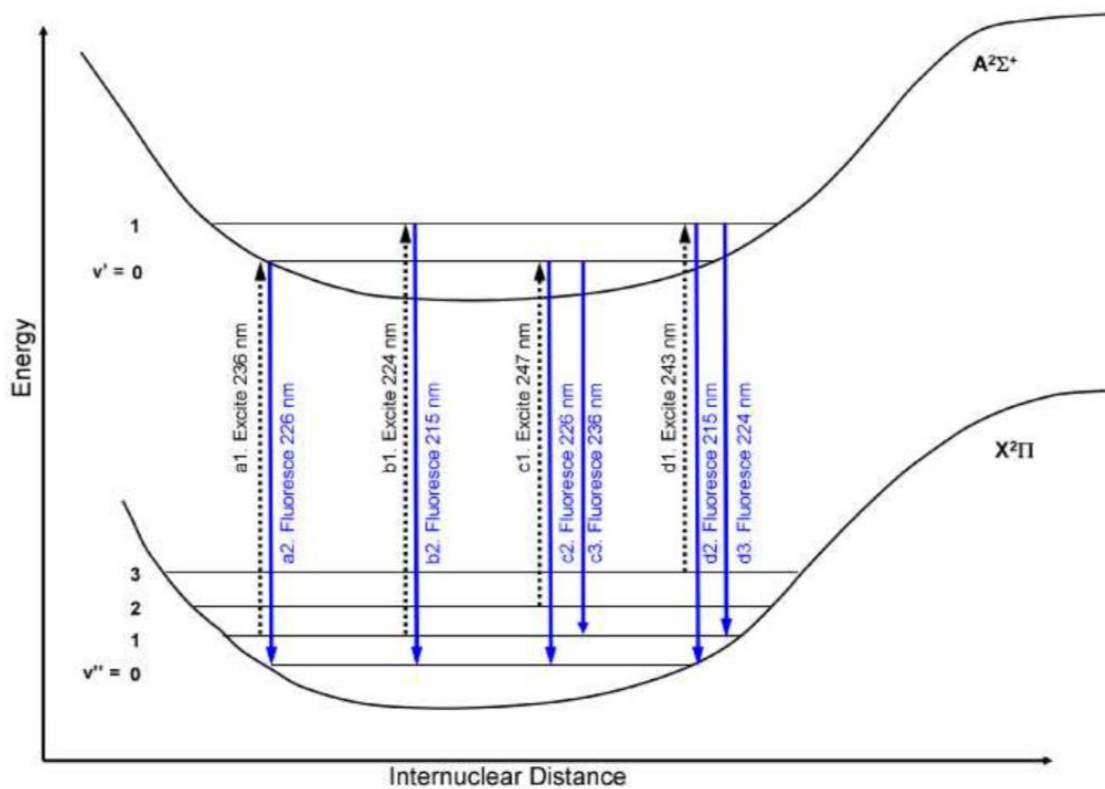


Figure 3. Energy state diagram

Depicts the transition between states caused by the exciting light listed and the return to the ground state after fluorescence.

Reproduced with permission.²⁰

²⁰ C. M. Wynn et al., "Noncontact Detection of Homemade Explosive Constituents via Photodissociation Followed by Laser-Induced Fluorescence," *Optics Express* 18, no. 6 (March 15, 2010): 5399, <https://doi.org/10.1364/OE.18.005399>.

CHAPTER IV – EXISTING SYSTEMS UTILIZED

The laboratory space and equipment utilized in the performance of this research were used for a similar project involving the measurement of radiation-induced ozone by means of Cavity Ringdown Spectroscopy (CRDS).²¹ In that research an existing vacuum chamber provided a controlled environment and enabled the user to shield or irradiate air mixtures as demanded. A tunable dye laser pumped by a pulsed Nd:YAG laser can produce collimated light within a wide range of wavelengths. The state of the entire experimental vacuum system is either controlled or monitored by a National Instruments compact reconfigurable input/output device, or cRIO. As the primary experimental system in the laboratory, the preliminary state of the existing system will be described in this section to help chronicle its evolution before modifications necessary for this work are discussed.

Vacuum System

The vacuum system was originally designed to simulate different atmospheric conditions for the study of radiation-induced fluorescence.²² It was modified in a later project to accommodate CRDS measurements with the installation of an internal optical cavity.²³ The most recent project added a quadrupole mass spectrometer to permit

²¹ Sidney Gautrau, “Cavity Ringdown Spectroscopy in Nitrogen/Oxygen Mixtures in the Presence of Alpha Radiation” 2016, https://aquila.usm.edu/masters_theses/258.

²² Aubri Capri Buchanan, *Characterization of Air Fluorescence Induced by Alpha Radiation* (University of Southern Mississippi, 2008).

²³ Reese, “A System for Measuring Radiation Induced Chemical Products in Atmospheric Gases Using Optical Detection Methods.”

calibrated measurements of trace gases with a detection limit of 1 ppm.²⁴ Figure 4 is a depiction of the vacuum chamber with labels indicating how each flange was used prior to the start of this project.

Physical Description & Port Usage

The vacuum chamber is a stainless steel sphere 18" in diameter featuring six 8.00", one 6.00", four 4.50", and eight 2.75" ConFlat style flanges radially focused on the chamber's center. Three 2.75" ports are used for monitoring internal pressure within the range 10^{-7} to 10^3 Torr. A single 2.75" port has an electrical throughput to allow the passage of thermocouple wire for measuring internal temperatures. One 2.75" port connects to a vent valve bringing the chamber up to atmospheric pressure without the use of specialty gases and for venting the chamber into the room in the event of accidental over pressurization to protect the integrity of the quartz viewports. A lower 2.75" port is connected to a pneumatic valve used for exposing the chamber to a roughing pump during evacuation.

²⁴ Gautrau, "Cavity Ringdown Spectroscopy in Nitrogen/Oxygen Mixtures in the Presence of Alpha Radiation."

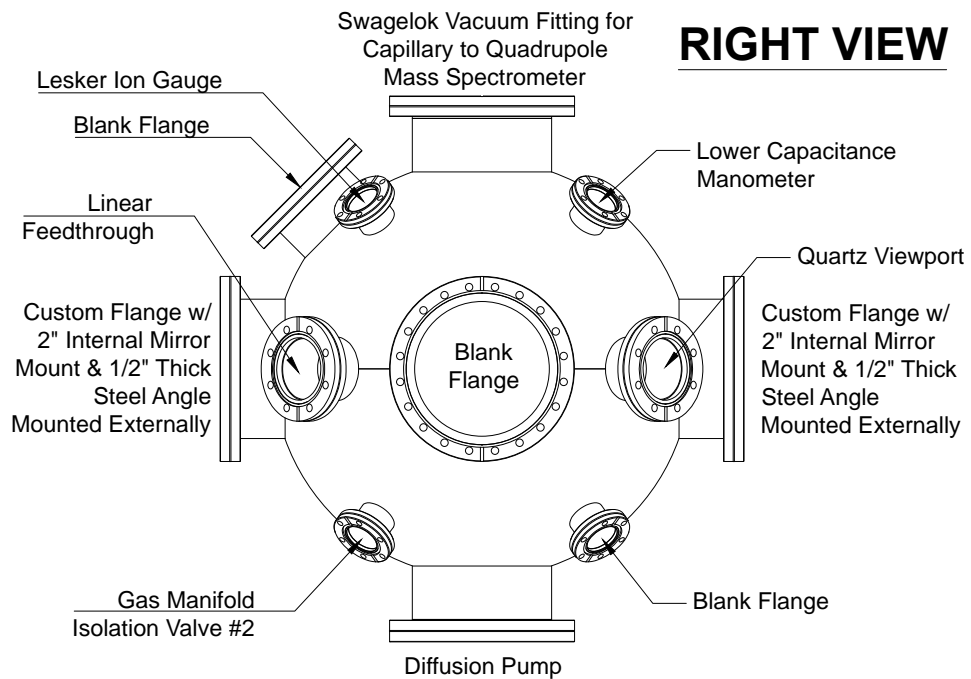
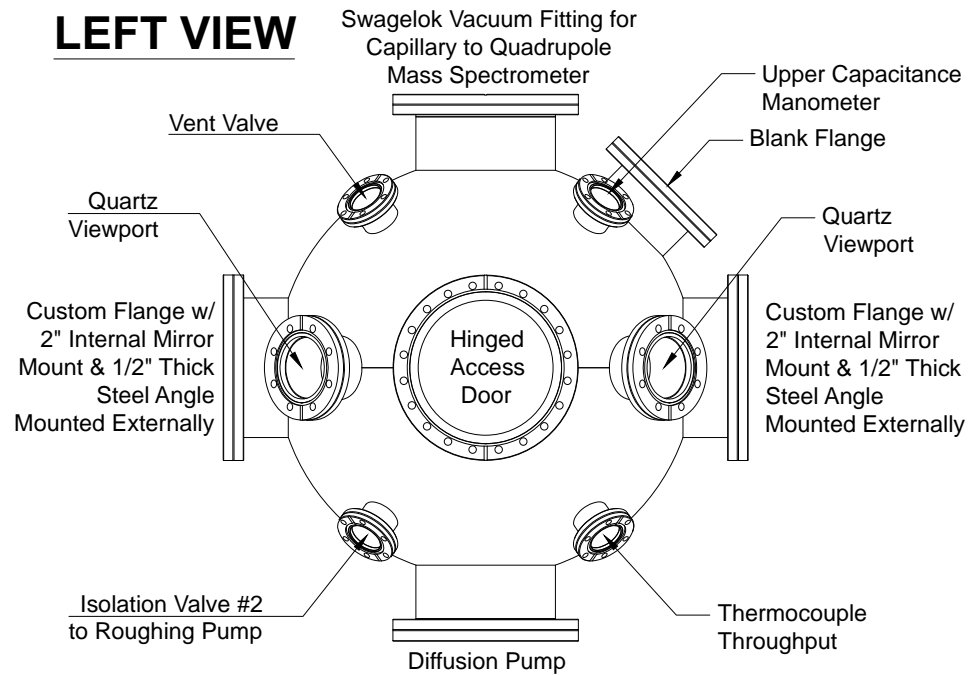


Figure 4. Initial configuration of existing vacuum chamber

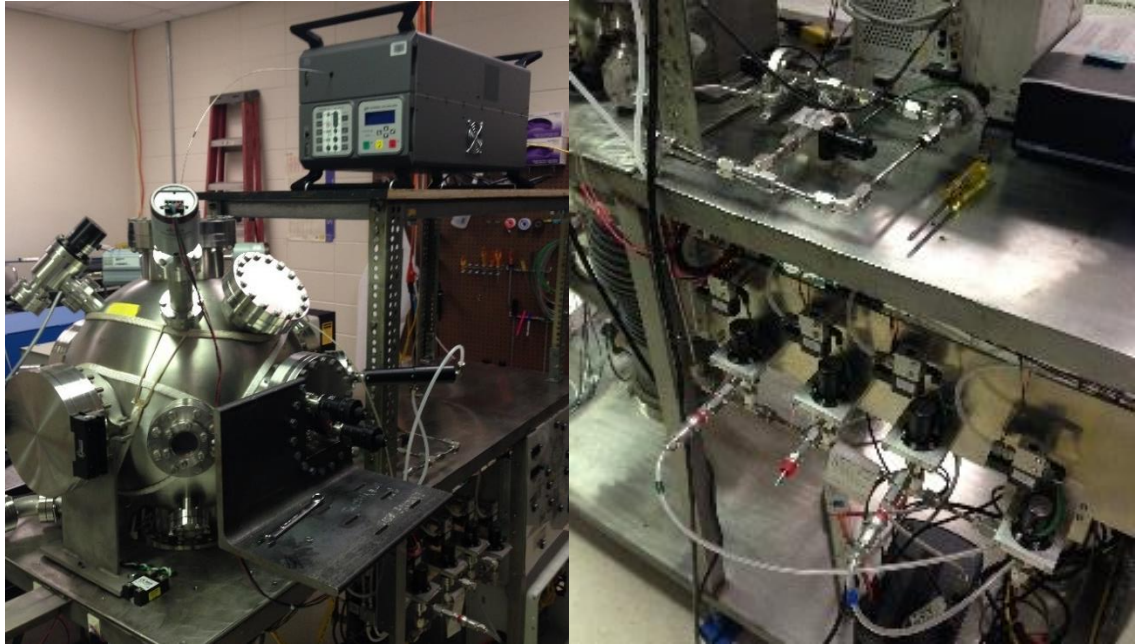


Figure 5. Vacuum chamber and gas introduction manifold

18" stainless steel vacuum chamber with components attached. Right: Gas introduction manifold, features three isolation valves for different gases, a metering valve, bypass valve, and manifold isolation valves isolating the chamber from the manifold. Photos by Sidney Gautrau. Reproduced with permission.

One 2.75" port is connected to a stainless steel gas introduction manifold isolated from the chamber by a pneumatic control valve. The manifold itself features three pneumatic valves used for the introduction of different gases to avoid contamination during flush and fill cycles. Downstream, an electric metering valve and pneumatic bypass valve are used for controlling flowrate. Quartz viewports mounted to three of the 4.50" ports allow laser-based measurements into the deep UV. A hinged door mounted to an 8.00" side flange allows access inside the chamber and keeps an airtight seal under vacuum. The 8.00" flange on bottom is bolted to a pneumatic gate valve to expose a diffusion pump and bring the chamber under high vacuum.

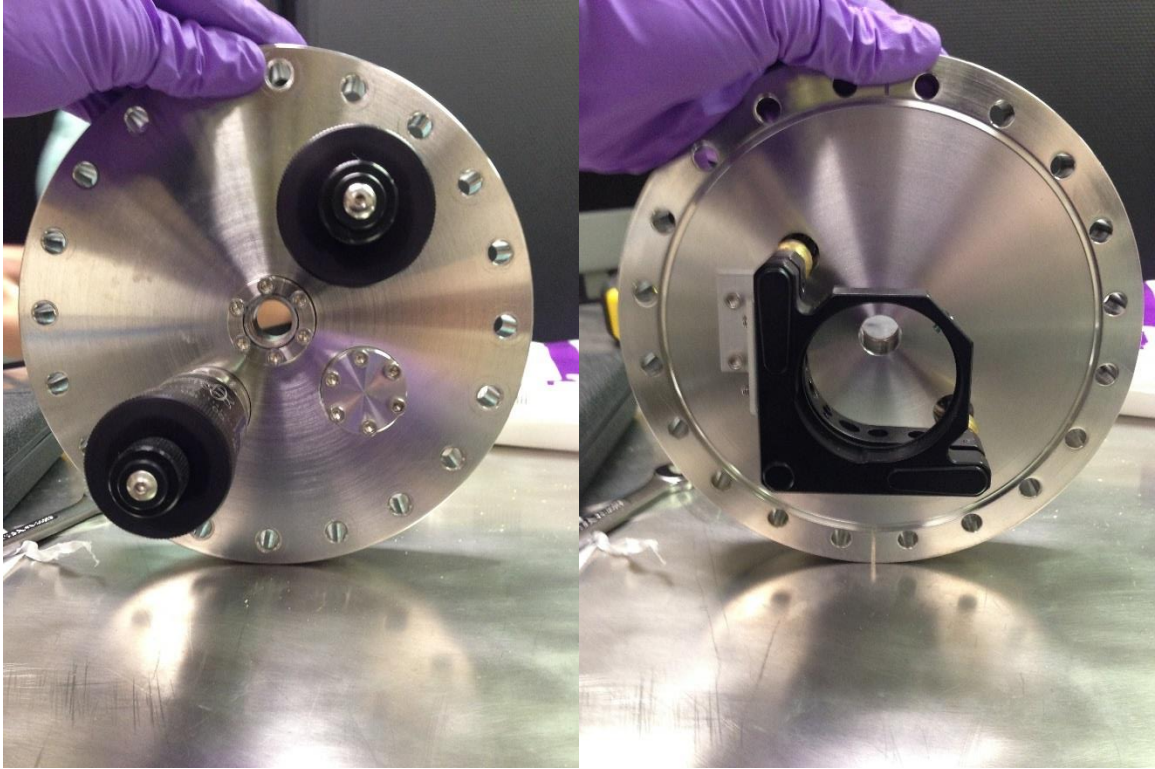


Figure 6. Custom 8” flanges for CRDS

Custom 8” flanges with 2” externally adjustable optical mounts used for CRDS. Photos by Sidney Gautrau. Reproduced with permission.

On 8” ports opposite each other, brackets machined from 0.5” thick angle iron support an optical breadboard for mounting various components. In addition, custom ConFlat flange caps have a 2” optical mount fastened to the inner face and a 1.33” quartz viewport in the center. Two rotary feedthroughs outside are linked to the optical mount adjusters inside by custom brass fittings to permit adjustment of the optical mount while the chamber remains sealed. Centered with each viewport, the 2” mounts face each other to form the “ringdown” cavity for CRDS measurements.



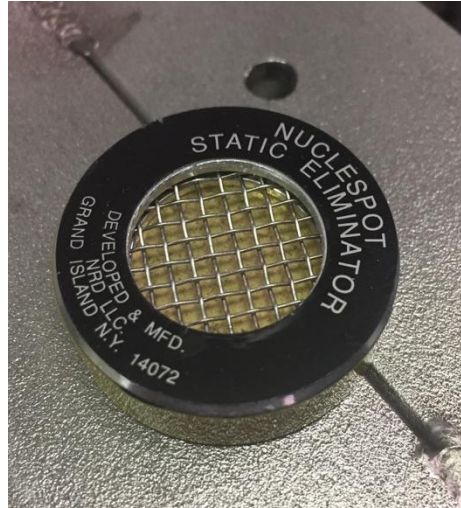
Figure 7. Original source holder and shield

Photo of the original aluminum source box, shield and extension arm inside the chamber. Photos by Sidney Gautrau and reproduced with permission.

The 8.00” flange located on top is bored through and tapped for a Swagelok fitting that provides a vacuum tight orifice for the UGA capillary. The inner face is bored and tapped so that two stainless steel threaded rods can support a stainless platform at the chamber’s center. An aluminum block bolted to the stainless platform is pocketed to encase two 1.5” diameter ^{210}Po alpha sources leaving the top face open to be covered by a retractable aluminum shield fastened to a linear feedthrough. The linear feedthrough is actuated by a 4-way pneumatic valve mounted to a 2.75” port 45° off axis from the “ringdown” cavity. The remaining 2.75”, 8.00”, and the 6.00” flange are capped and unused.

Figure 8. Polonium-210 alpha source

Two ^{210}Po alpha sources are used in all experiments requiring the presence of radiation. When new, they are 5mCi each and have a 138 day half-life.



Pumping Systems

The vacuum system is pumped down using up to three different pumps: two mechanical rotary vane pumps and a diffusion pump. The smaller rotary vane pump connects to the chamber with a flexible vacuum hose attached to a pneumatic isolation valve. This pump is capable of pumping the chamber down to pressures below 100 mTorr. A pneumatic gate valve attached to the bottom 8.00" flange isolates the diffusion pump from the spherical chamber. The diffusion pump is evacuated through the foreline by the larger rotary vane pump. The large rotary vane pump is separated from the foreline by a flexible vacuum hose attached to a pneumatic isolation valve. Once the pump is warm and the pressure inside the chamber is below 200 mTorr, the isolation valve for the small mechanical pump roughing the chamber must be closed before the gate valve can be actuated to bring the chamber atmosphere to near vacuum with pressures on the order of $10^{-6} - 10^{-7}$ Torr.

Measurement Capability

The vacuum chamber is fitted with several components that measure internal temperature and pressure. Upper and lower capacitance manometers and an ion gauge are attached to three of the upper 2.75” ports. The upper capacitance manometer has a range of 1 – 1000 Torr. The lower capacitance manometer has a range of 0.001 – 1 Torr. The ion gauge operates in the range 0.005 – 1×10^{-10} Torr. Two thermocouples measure the temperature of the chamber wall and internal atmosphere. The thermocouple wire is connected to the electrical throughput on one of the lower 2.75” ports. All measurement devices and thermocouples are monitored by a CompactRIO (cRIO) from National Instruments. A cRIO is a compact reconfigurable input/output device capable of monitoring and controlling several types of modules. Pressures and temperatures are displayed on the four LCDs mounted to the push button panel of the vacuum cart.

Control System

The vacuum system’s valves, sensors and thermocouples are completely controlled or monitored by a networked cRIO via its I/O modules. The cRIO is an embedded controller capable of processing data collected through its modules in real time. It is controlled through the network by a computer using National Instruments LabVIEW software. It can also be controlled without a computer by a custom push-button panel mounted to the vacuum cart. Mechanical buttons wired to digital I/O modules are monitored by the cRIO’s Real-Time application which autoruns on startup. A more thorough description of this application can be found in Gautrau’s work.²⁵

²⁵ Gautrau.



Figure 9. Electronics housing with cRIO

Project box housing the control electronics for the vacuum system: cRIO, attached modules and power supply, motor start relays, relays, terminal blocks, etc.

Laser System

Purchased in previous projects, the laser system consists of a pulsed Nd:YAG laser that pumps a high resolution dye laser with an attached frequency conversion unit (FCU). The Nd:YAG laser is made by Spectra-Physics and produces approximately 50 watts of power at the 1064nm fundamental wavelength. Its harmonic generator contains two crystals cut to produce second and third harmonics at 532 nm and 355 nm, respectively. Initially, the dye laser was pumped by the third harmonic to provide the energy necessary to pump coumarin dyes in the 400 nm to 460nm range.

The dye laser is made by Sirah and is tunable from 200 nm to 700 nm with the installed 2400 g/mm double gratings. The attached FCU must be utilized to double the fundamental output and reach the low UV wavelength mentioned. The dye laser also features a built-in wavemeter to electronically measure wavelength and automatically adjust the grating to control drift. The Nd:YAG laser is computer controlled through the

RS-232 interface using proprietary software. Alternatively, LabVIEW drivers are available to control everything with a custom LabVIEW virtual instrument (VI).

A 4' x 8' Newport optics table is situated parallel to the long dimension of the vacuum cart and provides a sturdy base to support the Nd:YAG and dye lasers. The pump beam is directed into the dye laser with 2" Y3 mirrors designed specifically to reflect the Nd:YAG laser's third harmonic. The mirrors and their mounts are housed underneath a black steel box adding protection against accidental bumps and hazardous reflections. The output beam of the dye laser is directed toward the vacuum chamber with an appropriate mirror coated for the selected wavelength. Polished aluminum mirrors in a vertical shift apparatus reflect the beam up to the height of the viewport on the chamber's 8.00" port. This port and the port opposite have a breadboard fastened to a custom angle bracket for mounting various optical components. These ports are primarily used for CRDS measurements.

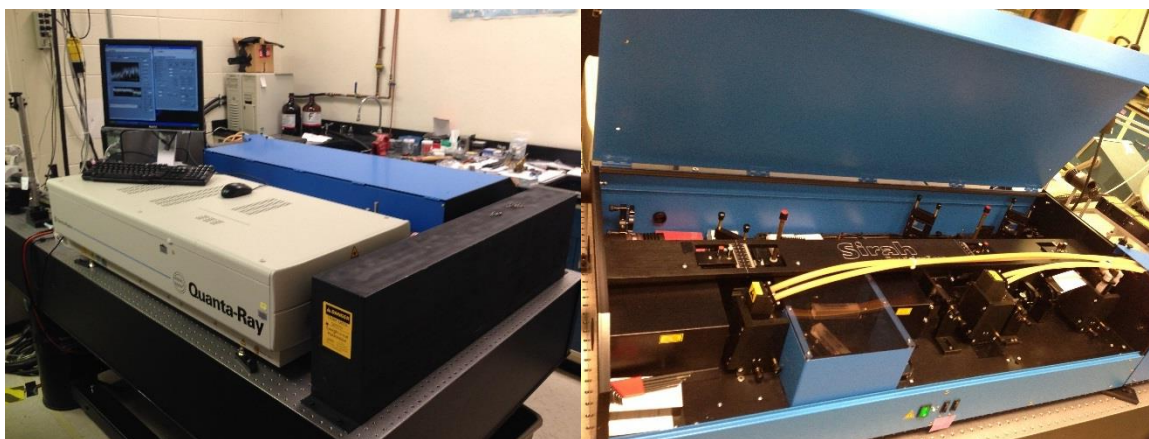


Figure 10. Nd:YAG and Dye lasers

Left: Nd:YAG laser mounted to 8' optics table. Right: Dye laser situated parallel with the Nd:YAG laser. Pictures by Sidney Gautrau and reproduced with permission

Data Acquisition System

A National Instruments (NI) PXI data acquisition system collects the current signal produced from a Hamamatsu 1P28 photomultiplier tube (PMT). A communication card in the first slot of the PXI communicates with a Windows XP computer through its PCI communication card. The second slot contains a data acquisition (DAQ) card which digitizes the signal received on each channel. Channel one is connected to the PMT, and trigger is connected to the Q-switch OUT port on the front panel of the Nd:YAG laser's power supply. Data collected and sent to the computer is processed by a custom LabVIEW VI. Data processing for this project is covered in detail in the software development chapter.

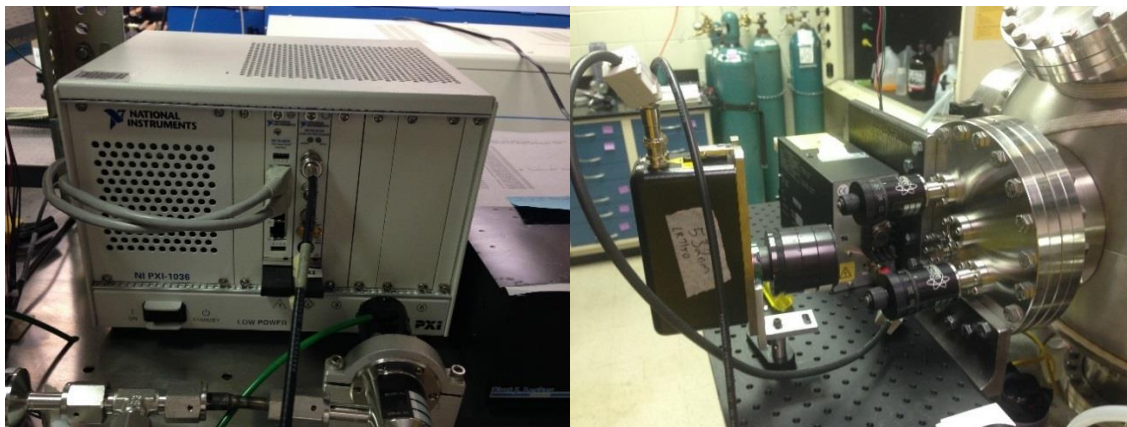


Figure 11. Existing data acquisition system

Left: PXI used for CRDS. Right: PMT housing with 1P28 tube inside used for CRDS. Photos by Sidney Gautrau. Reproduced with permission.

CHAPTER V – SYSTEM MODIFICATIONS

Modifications to existing systems were required to allow fluorescence measurements without loss of existing measurement systems. Changes to the vacuum system include integration of new components for added control over initial conditions and rearrangement of existing components to create the geometry necessary to conduct laser-induced fluorescence measurements. The laser system had to be reconfigured to permit sum frequency mixing (SFM) to produce a stable beam in the ultraviolet range for the purpose of eventually probing gas mixtures for NO. Additions to the control system help to increase the reproducibility of experimental results by allowing further control over experimental conditions. The data acquisition system was changed to achieve the temporal resolution and precision essential for accurate fluorescence measurements. This section covers the modifications for each system in detail.

Vacuum System Modifications

To create space for the LIF experiment and continue to accommodate the CRDS setup, the pneumatic piston responsible for opening and closing the source box was relocated to the 2.75” flange directly opposite. The quartz viewport on that flange was then moved to the piston’s prior location. This resulted in an optical path comparable to that of the CRDS arrangement with a viewport perpendicular to the LIF optical axis for collecting the fluorescence signal. The modified 2.75” cap mounted to a zero-length reducer on the chamber’s top 8.00” flange made an airtight passage for the UGA’s capillary tube. Since the UGA measurement capabilities are not currently required, the zero-length reducer flange was replaced with a quartz viewport to aid the initial

alignment of the experimental components the LIF system requires. A thorough description of each of the more substantial changes related to this system is given below.

New Source Box

A previous project measured ozone concentrations by CRDS. Ozone production rates measured experimentally were comparable to those calculated by Cantera.²⁶ Cantera is an open source chemical kinetics toolkit the research group uses to model production rates of chemical products produced by low energy collisions and to determine molecular species of experimental interest. Cantera also calculated production rates for nitric oxide.(see **Error! Reference source not found.**) From those calculations, it is suspected that the first five minutes of exposure are the most volatile with respect to the number density for ozone. To increase control and improve the accuracy of measurements collected during this time period, it was necessary to more effectively shield the air mixture from the radioactive sources by minimizing gas exchange while covered. Previous results suggest that leakage may have been occurring with the prior setup.

A box was designed to utilize the linear action of the pneumatic piston to pinch all four edges of the lid down with a relatively tight seal. The base features a pocket to keep the alpha sources recessed so that the lid can slide by smoothly. The sliding action is perpendicular to the plane of a dovetail profile that joins the base and lid. The wedge shape on the base and lid force the lid to pinch down tight as the pneumatic piston is actuated. This profile allows considerable clearance while providing precise alignment

²⁶ Chris Winstead, “2017 Annual Report DTRA” (The University of Southern Mississippi, 2017).

once fully pinched closed. The design also has a large surface area along its four sealing faces. The approved design was machined by the university machine shop using the more easily milled 304 stainless steel. To machine the inverse dovetail profile, the lid needed to be a three-piece design. The two dovetail profiles are bolted to opposite sides of the main lid with a Teflon film between the mating surfaces.

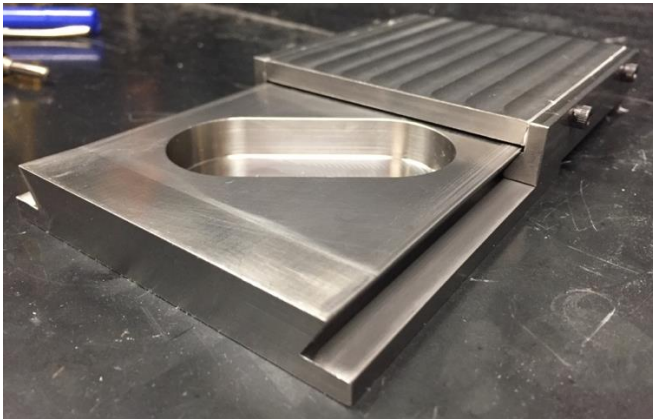


Figure 12. New radiation source box

304 stainless steel source box. The approximate position of the fully retracted lid is shown. The pocket allows two ^{210}Po sources to sit flush with the top of the base. The lid slides over the base and remains aligned because of the dovetail joint. The wedges on the ends of the base and lid reduce the clearance between the two pieces until the joint is pinched tight.

Extension Linkage

The pneumatic piston has 2" maximum travel; the lid of the new source holder requires a minimum of 3.5" to fully uncover both sources. It was therefore necessary to construct a linkage which translates 2" of linear travel into 4". The design, shown in Figure 13, is typical for most extender arms and uses 3 sections of identical dimensions. It is constructed entirely of 0.5" wide, 0.125" thick stainless steel with stainless rivets at each joint. The shared joint linking the first section to the second is anchored to the

platform at the center of the chamber. The first joint of the first section connects to the pneumatic piston and controls the extension of the last two sections. The anchored second joint is bolted to a 0.5” stainless optical post at one end which is bolted to a 0.75” wide, 0.75” tall, 0.125” thick piece of angled stainless steel. The opposite end of the stainless angle is bolted to the underside of the platform that supports the base of the box. The point where it is fastened was measured so as to set the fully retracted position of the lid. When the piston is fully extended, the lid is fully retracted to a position that completely exposes the sources and leaves the leading edge supported by the base. Once actuated, this configuration forces the last two sections of the linkage to extend and move the lid at twice the rate of the piston. Since the piston has 2” of travel and the lid only requires 3.5” to close, the lid is held closed tightly by the pneumatic pressure attempting to move the piston to its fully retracted position. Figure 14 shows the extender before being installed in the chamber.

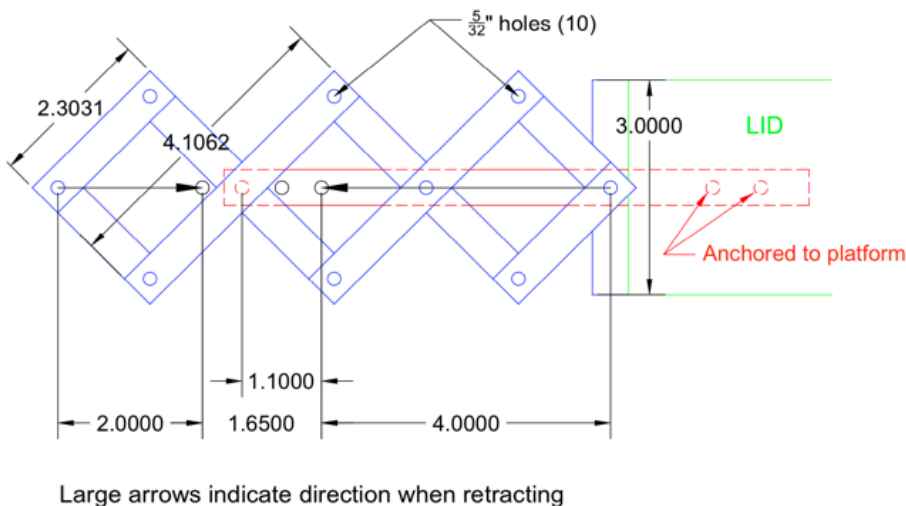


Figure 13. Extension linkage design for source box

CAD drawing displaying the dimensions and action of the extension linkage.

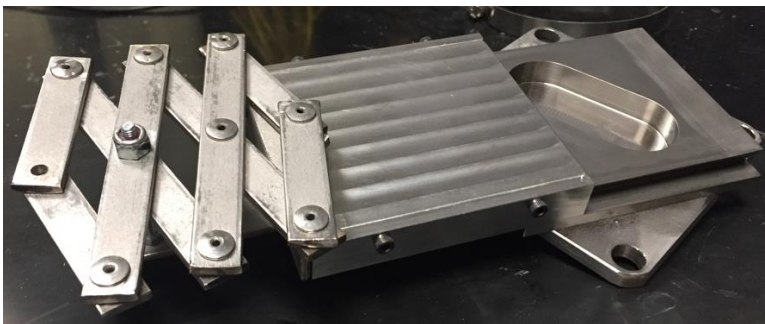


Figure 14. Extension linkage installed

All stainless source box with stainless steel extension arm attached. Translates 2" of horizontal range into 4".

Adjustable Platform Voltage

In previous work, decreasing the number of free electrons in the Cantera model resulted in a dramatic change to the simulated time evolution of the chemical product concentrations. This raised the question whether the stainless steel platform and supports are absorbing electrons and affecting the chemistry in the chamber. To study if electron absorption alters chemical reaction rates, it was necessary to electrically isolate the platform from the rest of the chamber. The two stainless support rods were cut near the top of the chamber. As shown in Figure 15, a female-female nylon union was used to rejoin the pieces. Nylon spacers and fasteners were used to attach the pneumatic piston to the extender arm to maintain isolation for components attached to the source cover.

The platform supporting the source box can be held at a constant electric potential after repurposing a glass braided thermocouple wire originally used for measuring the wall temperature inside the chamber. The wire was stripped to create a loop which was then sandwiched between two washers. The loop and washers were slipped over the stainless threaded rod support and tightened against the bottom of the main platform. The other end of the thermocouple connects to the electrical throughput located on one of the

lower 2.75” flanges. Outside the chamber, the electrical throughput connects the repurposed thermocouple to the terminal on a channel of an analog cRIO module. The corresponding ground terminal is connected to the vacuum cart to set the reference voltage. The voltage can be set within the range of ± 10 volts by adjusting the value of the “Platform Voltage” shared variable which is associated with channel 2 of analog output module 2 connected to the cRIO.

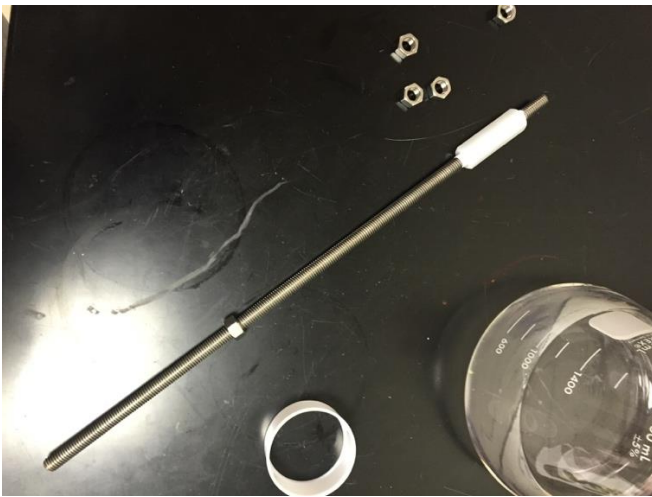


Figure 15. Electrically insulated stainless support

Three-eighths stainless threaded rod and nylon union used as an electrically insulated support for the source platform inside the chamber.

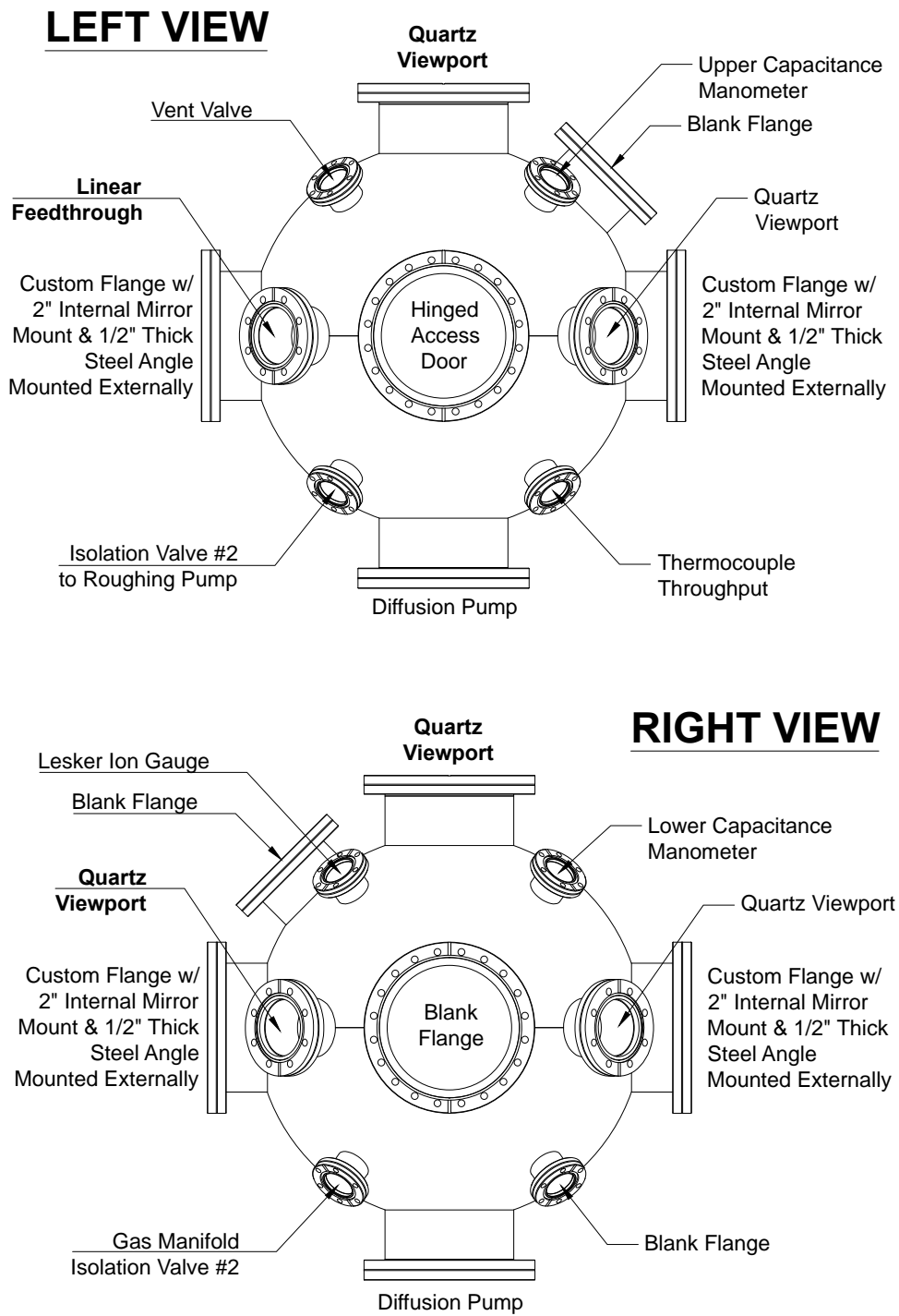


Figure 16. New configuration of existing vacuum chamber

Changes shown in bold

Control System Modifications

The control system was slightly modified from its previous state. A thermocouple was added to monitor the temperature of the Nd:YAG laser's infrared (IR) beam dump to increase the reproducibility of datasets. When the beam dump reaches 135°F the laser is considered at a steady state thermally and an experimental run can begin. To free a terminal on a thermocouple module connected to the cRIO, an unused thermocouple wire monitoring room temp was removed. As stated in the modified vacuum system section, a glass braided thermocouple wire monitoring internal chamber wall temperature was connected to the platform holding the source box. This allows it to be held at a constant electric potential to determine if electron absorption affects the chemistry.

Laser-Induced Fluorescence System

Laser System Modifications

The laser system was initially configured to use the third harmonic from the Nd:YAG laser to pump coumarin dyes in the pulsed dye laser. Coumarin is known for its short lifespan that shortens as pump energy increases. Frequency doubling the coumarin produced beam with the FCU proved inadequate. When frequency conversion efficiency is small, as it is in this case, the intensity of the frequency doubled beam is proportional to the square of the fundamental pump intensity.²⁷ This means when the power of the fundamental beam falls to half its initial intensity, the power of the second harmonic will have fallen to one quarter of its initial intensity. This would make measurements from

²⁷ Rudiger Paschotta, "Frequency Doubling," *Encyclopedia of Laser Physics and Technology*, accessed May 19, 2018, https://www.rp-photonics.com/frequency_doubling.html.

fluorescence experiments very difficult to make and reproduce within a reasonable range of certainty. To produce a powerful UV beam stable enough to work as a useful probe, the Nd:YAG laser's second harmonic is used to pump a red dye, while its third harmonic is sum frequency mixed with the red output from the dye laser.

Following the user manual, the Nd:YAG laser was reconfigured to produce both second and third harmonics. The harmonic generator (HG) was rotated 90° to generate a vertically polarized second harmonic necessary to efficiently pump the dye laser; this leaves the third harmonic horizontally polarized. Within the Nd:YAG laser's housing after the HG, 1.50" dichroic mirrors were installed in the configuration specified in the manual to separate the two wavelengths. The residual 1064 nm fundamental passes through the first dichroic immediately to a beam dump. The individual power output of both harmonics is maximized following the procedure outlined in the manual. First the second harmonic crystal is adjusted, then the third. At some point during revisions to the experimental system, the Q-switch for the Nd:YAG laser stopped opening automatically when using the wired remote control. It was discovered that it can be manually triggered by the Q-SW Trig IN on the power supply's front panel. A function generator now opens the Q-switch $197\mu\text{s}$ after receiving a TTL pulse from the lamp sync OUT terminal as specified in the laser manual. Alternatively, the Nd:YAG laser can be operated using virtual controls within the proprietary GCR software which does not inhibit the automatic Q-switch actuation.

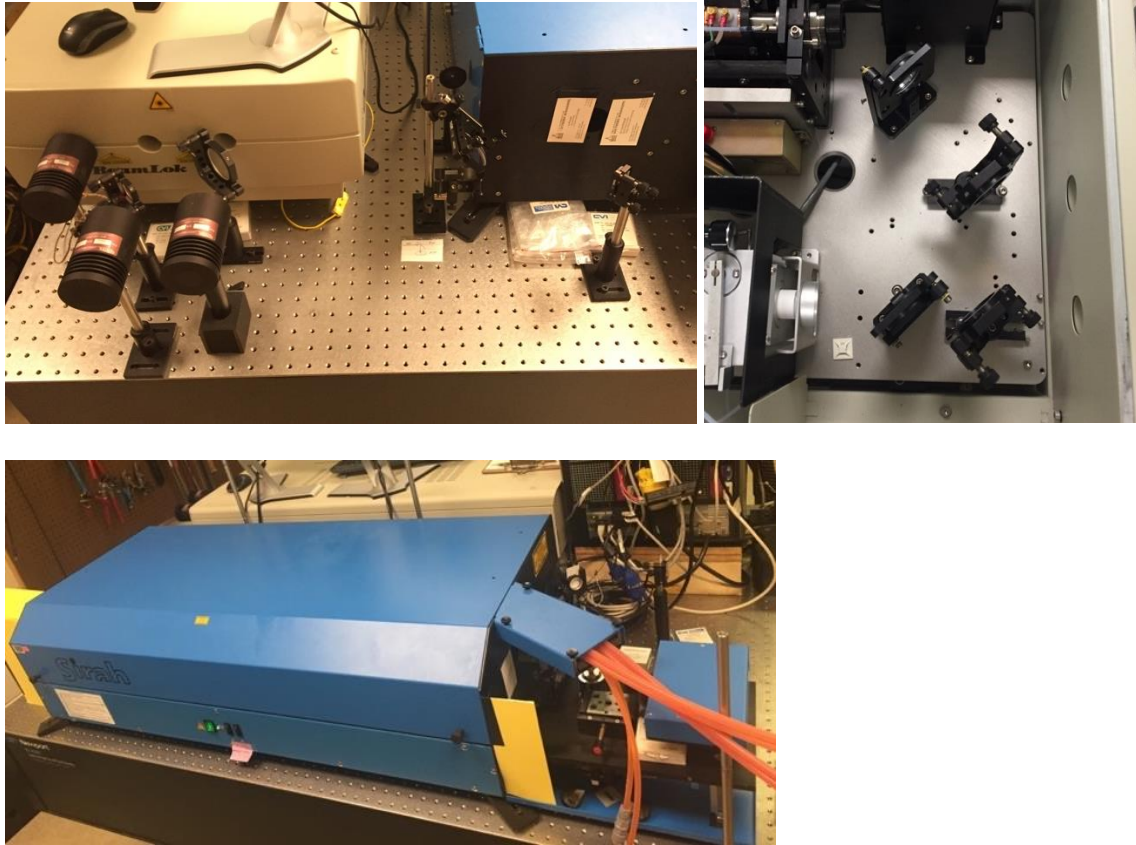


Figure 17. Modified dye and Nd:YAG lasers

Top Left: Beam dumps and mirror arrangement between the Nd:YAG laser and dye laser. Top Right: 1.5" dichroics inside the Nd:YAG laser housing used to separate the fundamental from the harmonics, and the third harmonic from the second. Bottom: Modifications to the dye laser's FCU housing necessary to implement sum-frequency-mixing.

It was determined that LIF will be used to detect NO experimentally to help validate the computational model. NO fluoresces strongly near 226 nm. To reach the 226 nm range, the Nd:YAG laser's third harmonic must be mixed with the output of a red dye capable of producing 623 nm light. A solution of DCM dye in ethanol was selected for having the highest conversion efficiency as cited by the dye laser manufacturer. A complete realignment of the optical components within the dye laser was required after the decision to pump with the Nd:YAG laser's second harmonic. The laser was then

calibrated to within 30 pm using the spectral lines of Argon following the procedure outlined in the user manual. The dye laser was not designed to easily accommodate sum/difference frequency mixing. It was therefore necessary to remove the side panels on the attached frequency conversion unit (FCU). The section that follows describes all modifications and procedures necessary to adapt the FCU for frequency mixing.

Sum Frequency Mixing

Frequency mixing is a phase-sensitive process meaning both photons must have the same polarization and refract through the crystalline face with a specific angle of incidence. Since the output of the dye laser is vertically polarized, the third harmonic must be rotated 90°. This is accomplished by using a Y3 s-type mirror to reflect the beam down with a 45° angle of incidence in the X-Z plane. The beam then reflects off a p-type Y3 mirror with a 45° angle of incidence in the Y-Z plane. Figure 18 provides a visual reference for the polarization rotation described.

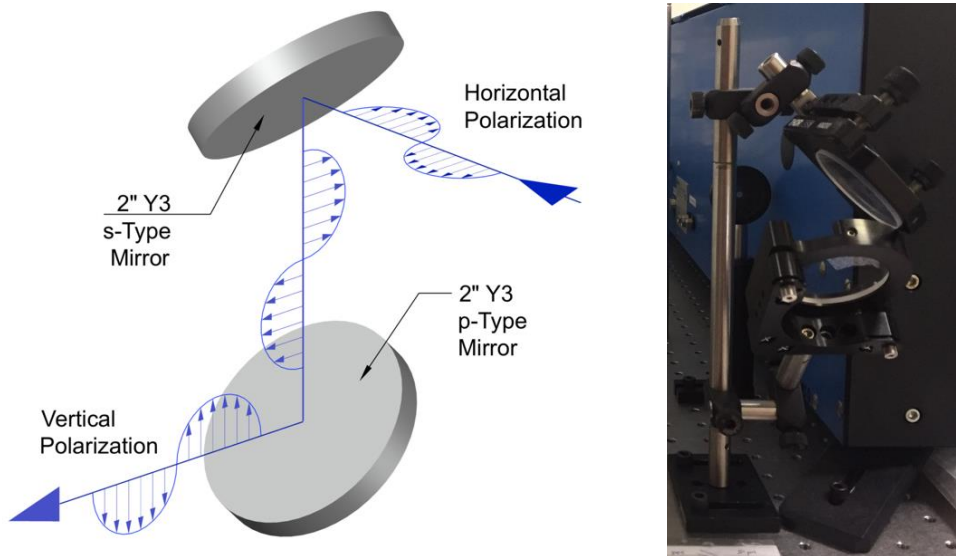


Figure 18. Polarization Rotation Diagram

Depicts the mirror arrangement used to rotate the polarization of the Nd:YAG laser's third harmonic.

The rotated beam is sent horizontally across the table between the dye and Nd:YAG lasers. A 1" TLM1-350 s-type mirror is placed in the path of the dye laser output beam to act as a dichroic for superimposing the two beams. The 355 nm UV beam is adjusted so that it strikes the mirror at the same point the 623 nm red beam is transmitted. The mirror mount is then adjusted so that the red and UV remain superimposed when viewed on a screen approximately six feet away.

When pumping the DCM dye solution, it takes time for the population inversion and subsequent emission of the laser pulse to occur. To compensate, the travel time for the third harmonic pulse must be extended. Using an oscilloscope and a fast response photodiode triggered by the Nd:YAG laser's Q-Switch, the difference in arrival times is found by placing cursors at the peak of each pulse. The delay between pulses was measured using a short and direct path for reference. The path length for the third harmonic was then calculated and extended utilizing three additional Y3 mirrors. The procedure for superimposing the beams was then repeated. The translation stage for the FCU stepper motors is adjusted so that the shafts are aligned with the superimposed beam path. The beta Barium Borate (BBO) crystal and its compensator were then installed onto their respective stepper shafts.

To combine a 355 nm photon with a 623 nm photon, the two must have a 59.1° angle of incidence with the crystalline face. The BBO crystal used is cut at 57.4° . This means the angle of incidence is 57.4° when the windows of the BBO housing are perpendicular to the beam path. The stepper can be adjusted $\pm 45^\circ$ from the central position to produce the incident angle required. Since the stepper motor takes 708,000 steps to move through its full range of 90° , the additional 1.7° of angle necessary can be

calculated in terms of steps. If 57.4° equals 354,000, then 59.1° equals 367,373. This position provided a starting point for which to visually detect the 226 nm beam. During this procedure the first Pellin-Broca prism of the wavelength separation unit was used to separate the individual beams and image them onto a screen to help identify the resultant UV.

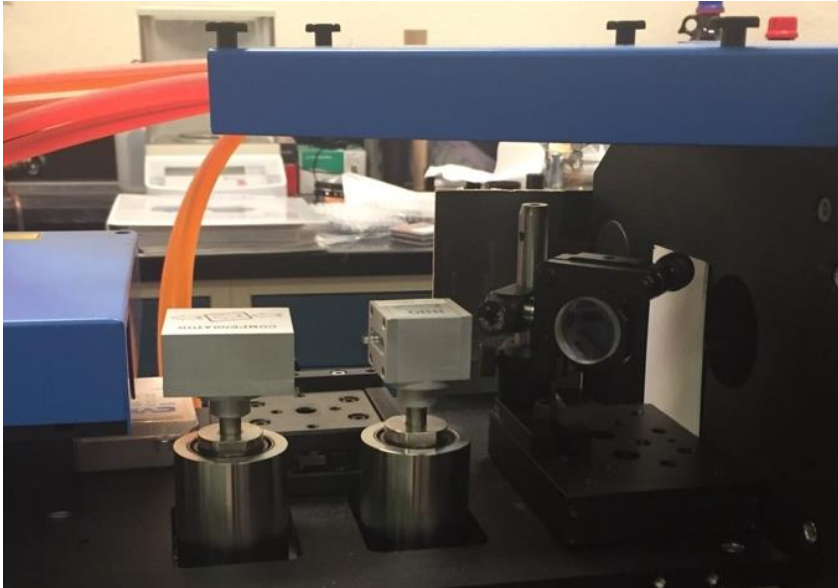


Figure 19. FCU: BBO, compensator, and dichroic

Left to right: compensator, BBO, 350TLM1 mirror used as a dichroic

The wavelength separation unit was installed and the Pellin-Broca prisms inside were adjusted so that the 226 nm beam refracts through all four before exiting the FCU housing. The beam then makes a 45° angle of incidence with a Y5 mirror aligned with the centerline of the chamber. A spectrometer was used to aid with optimizing the FCU motor position at each wavelength interval. The frosted glass tip of the spectrometer's fiber optic is placed in the path of the resultant UV beam. The spectrometer's proprietary software gives the user a photon count at the wavelength selected. Using the *Sirah*

Control software, the stepper motor position is fine tuned to maximize the photon count. The optimum position is recorded in a table the laser software uses to map FCU motor position to fundamental wavelength. This process is repeated for several points ranging from 225.9 nm to 227.1 nm, the results of which are in Table 2. Experience after completing this process several times suggests that three points is sufficient over a narrow bandwidth such as this. Additional points become redundant and the process time consuming.

Table 2 *Wavelength vs. Motor Position*

Fundamental Wavelength	FCU Motor Position
623.0	370700
626.5	363670
630.0	356730

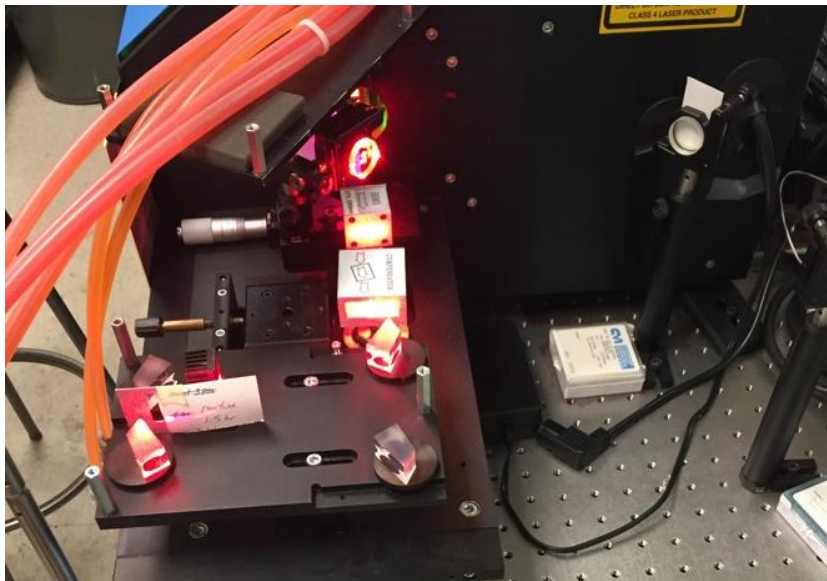


Figure 20. FCU: Wavelength separator

Wavelength separator composed of four Pellin-Broca prisms designed to separate the individual beams used for mixing from the resultant beam while controlling drift caused by FCU motor adjustments.

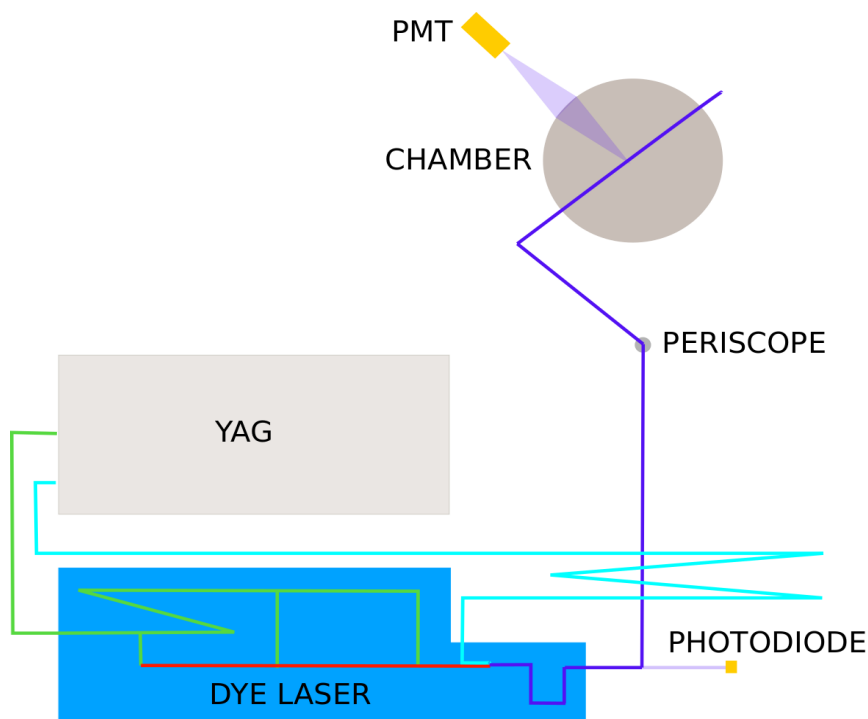


Figure 21. Laser system path

Depicts the path of the laser beams from each laser and the resulting UV used for fluorescence measurements. Green (532 nm), Blue (355 nm), Red (~623 nm), Purple (~226 nm)

Dark Room

The dark room is necessary to shield the PMT from room light thereby increasing the signal-to-noise ratio which helps make the experiment as sensitive as reasonably possible. A 12" x 12" optical breadboard is bolted to the existing 8" x 24" breadboard mounted on the output side of the custom 8.00" flanges used for CRDS experiments. One edge of the new breadboard is supported by optical posts resting on the cart and the existing breadboard bolted to the 0.5" thick angle bracket supports an adjacent edge by 1/4-20 threaded bolts. It creates a sturdy platform directly in front of the adjacent viewport window to provide a place to mount the lens and PMT for the fluorescence signal collection and detection. The 2" diameter UV compatible lens is secured in a 2" lens

mount placed flush with the viewport window to maximize the internal viewable area. Heavy cardboard painted black and black vinyl tape are used to create three walls of the dark room, cover the breadboard holes underneath, and seal all pinholes that allowed room light inside. The top and outer wall of the room is made of black optical cloth for easy access.

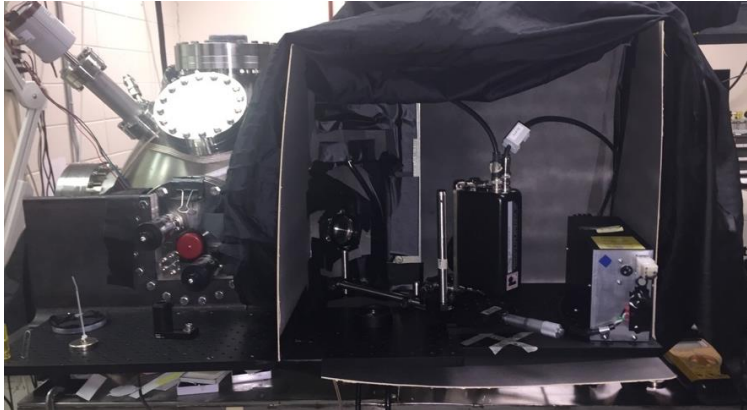


Figure 22. Dark room

DAQ System

The existing data acquisition system lacked the sample rate necessary to capture a fluorescence signal. A Tektronix TDS3054B four channel oscilloscope was incorporated for its 5 GS/s sample rate. It is controlled by a custom LabVIEW VI capable of capturing up to four waveforms per second through its Ethernet port. It is set to acquire and average 32 waveforms before transmitting to the computer. A battery-powered fast-response photodiode is connected by BNC to channel one of the oscilloscope. It is placed behind the first turning mirror immediately after the FCU housing to collect the transmitted portion of the UV beam exiting the wavelength separation unit as shown in Figure 23. A Hamamatsu PMT model 1P28 is used to collect the fluorescence signal and is connected

by BNC to channel two of the oscilloscope. It is powered by an adjustable power supply providing 500 – 1200 volts between the first and last dynodes. Prior to installing the PMT, the distance from the lens to the center of the chamber was measured; a screen was placed the same distance away from an illuminated object until a focused image was produced. The image distance was used to find the approximate location to place the PMT. The PMT is mounted on a translation stage to easily and smoothly adjust its position relative to the lens. This step ensures the image visible through the lens is in focus at the PMT to allow the use of slits or blinds.

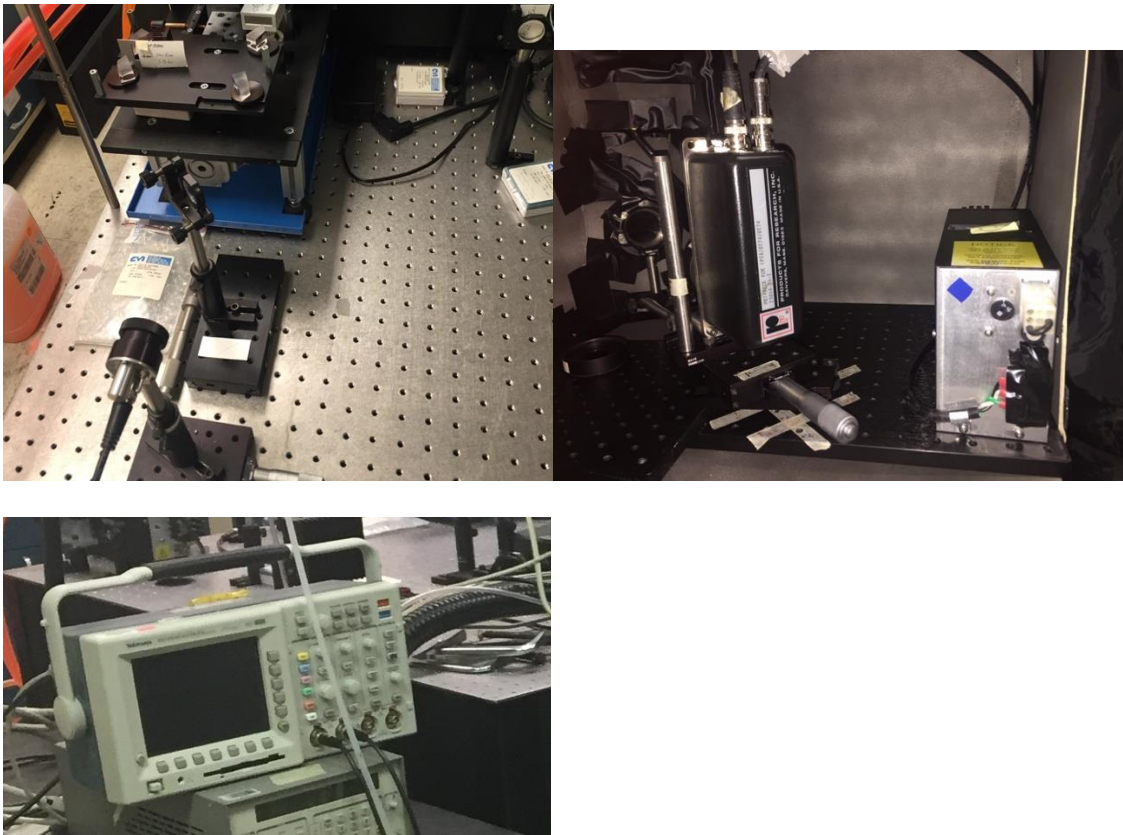


Figure 23. Data acquisition system

Top Left: battery powered photodiode used for measuring the power of each pulse. Top Right: PMT and power supply used to collect the fluorescence signal. Bottom: Tektronix 3054B oscilloscope used for data acquisition.

CHAPTER VI – SOFTWARE DEVELOPMENT

In previous work which documented the evolution of this experimental system, the dye laser and cRIO were directly controlled by one computer running LabVIEW 2014 SP1, while ringdown measurements and sensor data were recorded by another running LabVIEW 2009 SP1.²⁸ This was necessary because the LabVIEW 2014 software required by the cRIO executes the *ringdown time* VI at half the rate of LabVIEW 2009 SP1. By taking advantage of LabVIEW's shared variable engine, SVE, the two computers and cRIO worked together through the laboratory network via the SVE's publish-subscribe protocol, or PSP. For each computer, shared variables were created for everything that needed to be either monitored or controlled from the other computer. To minimize lag from high query rates to the SVEs, *while* loops monitored the other computer's variables and wrote their values to local variables that could be read by the local VIs. Changes that needed to be made to control states would write directly to the PSP shared variable. In practice, this configuration would sometimes lag and either slow or stall execution of the *ringdown time* VI, which is responsible for recording all sensor data and ringdown measurements to a spreadsheet file. In addition, operating system choices have been limited to Windows XP, in part, due to incompatible drivers for a PCI to PCMCIA adapter card. This adapter is required to make use of a PXI-8310 PCMCIA card to communicate with the PXI-5124 digitizing module attached to the PXI-1036 chassis. By changing the DAQ system from the PXI-1036 to the four channel TDS3054B Tektronix

²⁸ Gautrau, "Cavity Ringdown Spectroscopy in Nitrogen/Oxygen Mixtures in the Presence of Alpha Radiation."

oscilloscope, this configuration could change. The existing *dye laser control* and *ringdown time* VIs were modified to facilitate the use of a single computer to control the entire experimental system. This section will detail changes to the laboratory computer network and the features and modifications of each VI.

Laboratory Network

The laboratory network is a closed network, with no direct connection to the USM intranet or internet. A Netgear wireless router is at the core of the private network and connects all Ethernet capable devices attached to the experimental system. It works as a hub to allow communication between two Windows XP computers, the Tektronix oscilloscope, and wireless clients. One of the XP computers controls the dye and Nd:YAG lasers and is directly connected to the NI cRIO-9066 through a secondary Ethernet adapter; the other is no longer used but remains connected. The cRIO controls the vacuum system and monitors all of its sensors. Two Windows 7 computers in the lab office are authorized to connect to the router wirelessly to allow remote operation of the system and access to datasets that are saved on the XP computers. A visual representation of the network is shown in Figure 24.

Since Windows XP is no longer supported by Microsoft, security exploits from direct connections to the internet could potentially compromise the computers responsible for running the experimental system. The router's built-in firewall rejects all unrequested outside traffic from being distributed within the private network. By using the Windows 7 computers as intermediaries, the network is better protected from viruses and other malicious programs. The router is configured with static IP addresses for the two Windows XP computers and Windows 7 machines to standardize routes within the

network and computer identification for remote access. All other connections are assigned IPs by the router's DHCP server. Unauthorized access and outside visibility of the wireless network is minimized by securing it with WPA2 encryption and keeping the router SSID hidden.

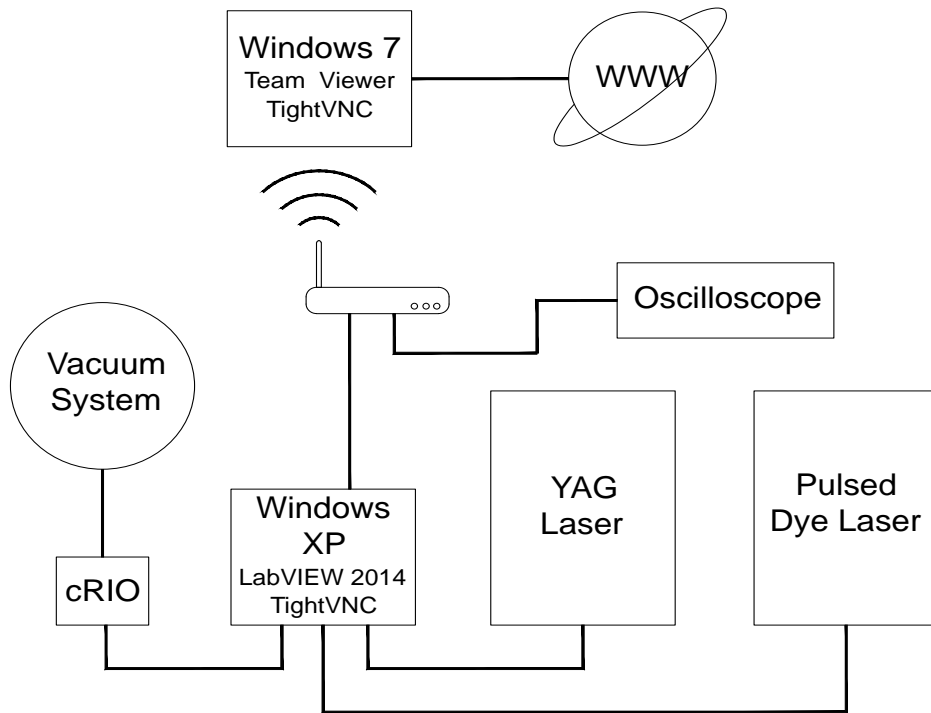


Figure 24. Laboratory network diagram

Diagram depicting the laboratory network and how each system is linked.

The Windows XP computer serves as the nexus of control for the entire experimental system. It is connected to the pulsed dye laser by a straight-through female-to-female RS232 serial cable. The laser's built-in wavemeter is monitored by an EPIX D2X1 PCI camera card through the provided cable. The dye laser can be controlled using Sirah's proprietary *Sirah Control* program or by user created VIs via the supplied LabVIEW drivers. A PCI-e serial card offers two additional serial ports to the machine. One of these ports is connected to the Nd:YAG laser by a male-to-female RS232 straight-

through cable. The interface allows remote control of the laser through the Spectra Physics GCR software and provides diagnostic information about the system for troubleshooting failures. This computer is also directly connected to the NI cRIO-9066 using a secondary USB-to-Ethernet adapter and crossover cable. The connection is auto-configured by the National Instruments *Measurement & Automation Explorer*, or MAX.

The modules connected to the cRIO-9066 are directly wired to every valve, thermocouple, sensor, pump, LCD and push button associated with the vacuum system. The XP computer controls the cRIO through shared variable libraries included in the *Vacuum System Control.lvproj* LabVIEW project file located on the XP's desktop. The cRIO can monitor and control most of the vacuum system components without using a networked computer through the attached push button panel. It uses LabVIEW 2014 SP1 to run a Real-Time autostart application generated from a VI designed to allow autonomous control and monitoring of the system and to continuously check for alarm conditions. The panel features a cartoon image of the vacuum system with labelled mechanical push buttons at the approximate location of the valve or pump they each control. The panel also features four LCDs to display the pressure or temperature selected by a three-way toggle switch adjacent to each. For a more detailed description of the Real-Time application the cRIO runs, see Gautrau's work.²⁹

Control Software

The LabVIEW programming environment was used to build several VIs which control and monitor the experimental system. LabVIEW (Laboratory Virtual Instrument

²⁹ Gautrau.

Engineering Workbench) is an object-oriented programming language by National Instruments (NI) which graphically represents functions, variables, loops, indicators, etc. All programs created consist of a front panel and block diagram. The front panel is the customizable user interface where all controls and indicators are placed. The block diagram is where the graphical source code is written. LabVIEW programs are called virtual instruments (VI) since the collection of controls and indicators on the front panel resemble physical instruments in form and function. Several VIs used in the conduction of this research have been used in previous projects. Parts from an existing VI were used to build a new VI capable of collecting both LIF and CRDS measurements simultaneously. An existing VI that controls the vacuum system was modified to control the voltage of the platform supporting the alpha source box and monitor the temperature of the Nd:YAG laser's IR beam dump.

"Vacuum System Control.vi"

The vacuum system control VI is mostly unchanged from its previous version. On every iteration of the VI's main while loop, the state of the buttons located on the *Controls* tab are updated to reflect the values of the shared variable boolean array *ControlsState*, which is set only by *ControlsSubVI.vi*. When a button on the *Controls* tab is pressed, a boolean array indicating the state of every button on the front panel is sent directly to *ControlsSubVI.vi* to request the desired change to the system. If the requested change passes the logical conditions set for the particular action, the change to the system is made and the *ControlsState* boolean array is updated. The buttons on the front panel of the *Controls* tab then update to reflect that change. If the conditions are not met, the requested change will not occur and the button will return to its previous state.

ControlsSubVI.vi will also write any changes made to the system as a string to the shared variable *Status*. If the change does not occur due to not passing the logical conditions set, “CONDITIONS NOT MET” will be written followed by the name and state of the control that failed to change. Each change is appended to the existing value of *Status* along with the timestamp for when the change was made or attempted. The value of *Status* is visible on the *Controls* tab in the *Status/Alarms* field. The Real-Time application the cRIO runs also uses *ControlsSubVI.vi* to make changes to the system. In this way, changes to the system requested from the vacuum cart push panel must pass the same logical conditions as those from the computer. The state of the buttons on both panels and the *Status/Alarm* field on the *Controls* tab of *Vacuum System Control.vi* will also reflect changes made by either. The *Status/Alarm* field can be cleared by pressing the *Reset Status/Alarms Report* button; its contents are saved to a text file in a folder located on the desktop using the current timestamp as the filename.

There are four numeric fields below the *Status/Alarm* field that indicate pressure readings from the ion gauge, diffusion pump foreline, and upper and lower range manometers. Two more fields were added since the previously documented version; one that sets the voltage of the platform inside the chamber and one that indicates the temperature of the Nd:YAG laser’s IR beam dump. On startup, the platform voltage field is set to the value of the shared variable *Platform Voltage*. An event structure on the block diagram waits for a change to be made to this field, then updates the *Platform Voltage* variable. *MIV2 Filler* button should be used to help prevent over pressurization of the chamber and to simplify gas fills for the user. When the *MIV2 Filler* button is

pressed, manifold isolation valve #2 will automatically open to fill the chamber with gas then close once the pressure entered in the *Filler Set Pressure* numeric field is reached.

The *Automated Task* tab contains two automated tasks; *Cycle Control* and *Rad Source Cover Control*. For reference, there are fifteen LEDs on the left-hand side of the tab that display the state of the controls listed on the *Controls* tab. *Cycle Control* uses *CycleControlSubVI.vi* to automate the vacuum and fill cycles needed to flush the chamber before filling with the desired gas. The subVI opens and closes the necessary shutoff valves in the proper sequence and at the proper time to simplify and standardize the fill process of each experimental trial. Roughing pump #2 must be running prior to starting *Cycle Control* task as indicated by the caret beside its indicator. If the diffusion pump is to be used during the pumpdown cycles, the *Use Diffusion Pump* option should be selected. When using this option, roughing pump #1, #2, and the diffusion pump should be on with isolation valve #1 open as indicated by the asterisk next to each indicator. The three numeric control fields set the number of vacuum-fill flush cycles to execute, the pressure to reach during fills, and the duration to remain at vacuum after each pumpdown. The *Cycle Gas* radio button selects the gas to use for the flush fills. The *Sample Gas* radio buttons selects the gas to use for the final fill. The percentages set for *Sample Gas 1a* and *2a* define the mix of the final fill. This feature is useful when diluting the gas of *1a* is desired. The *Cycle Control* task starts once the square *GO* button is pressed. The *Rad Source Cover Control* is used to open and close the rad source lid for a predefined number of intervals. Each cycle is an opened and a closed state for the duration specified. It can be set to start in the open or closed position.

The *Maintenance* tab contains several numeric indicators that display the runtime hours and number of start cycles for the three pumps and the laser power supply. These counters can be reset using the reset buttons beside each group of indicators. The three text fields set the labels associated with each gas shutoff valve. These labels must be set as the default value each time they are changed or else they will revert to their previous value next time the VI is opened.

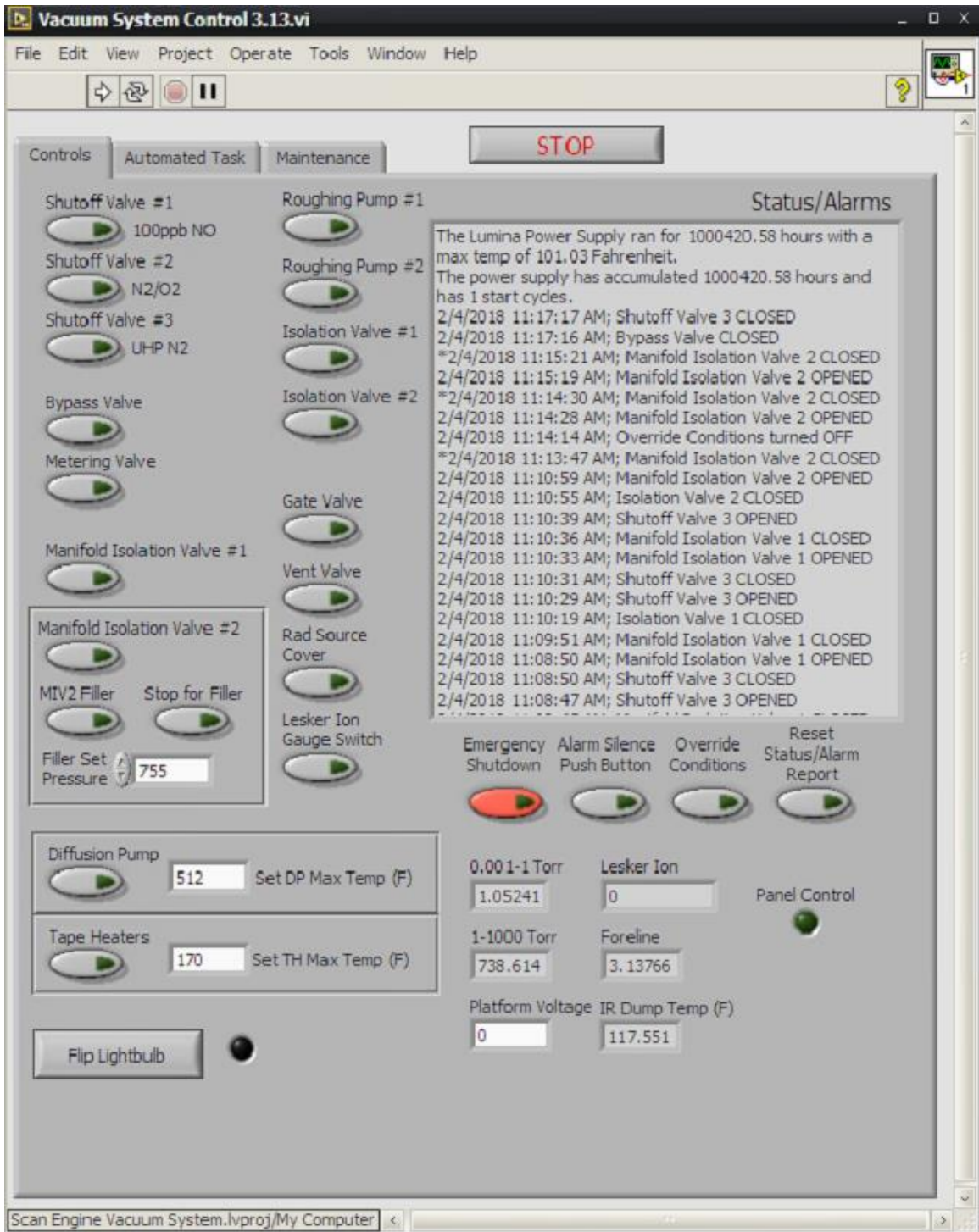


Figure 25. "Vacuum System Control.vi" Controls tab

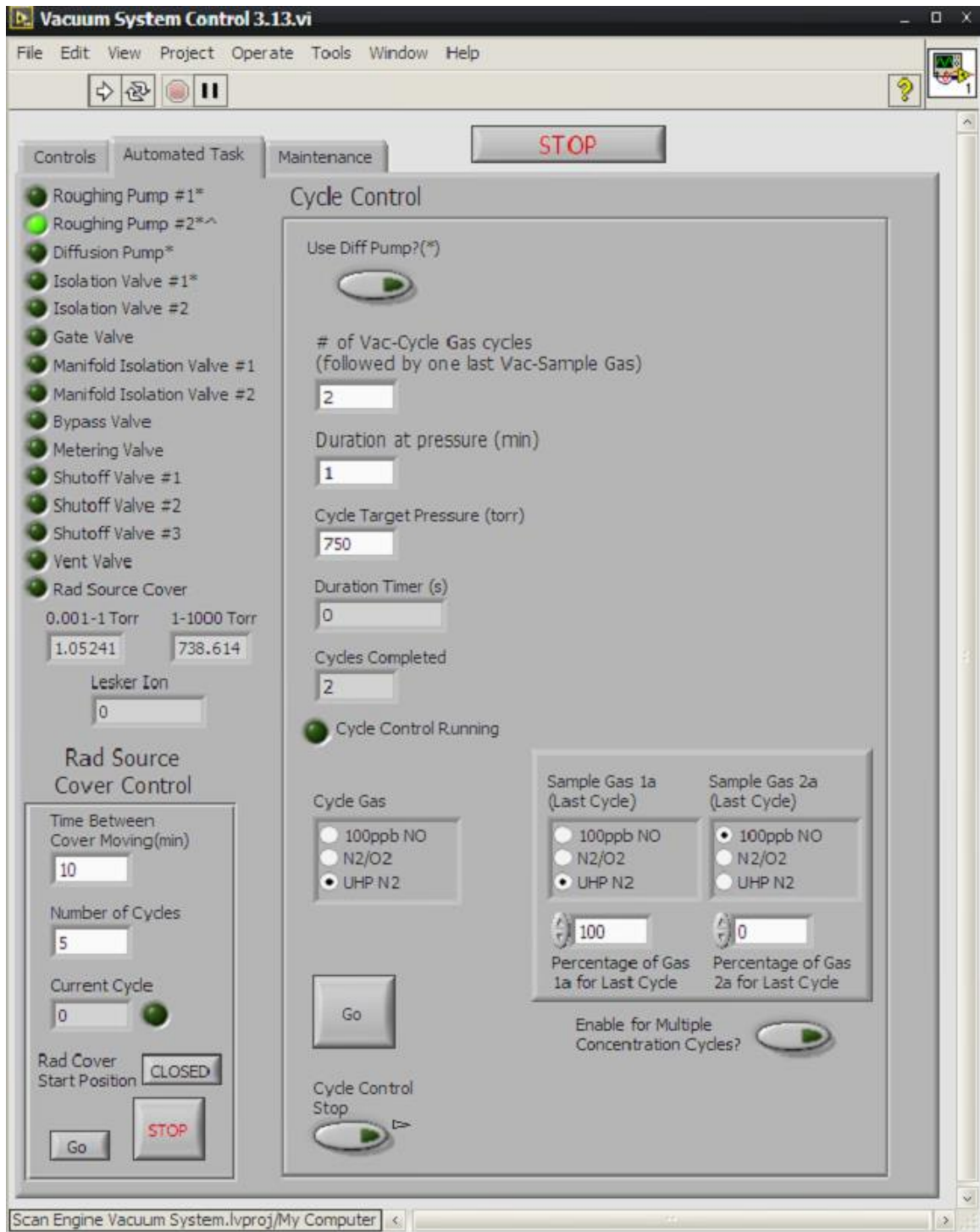


Figure 26. “Vacuum System Control.vi” Automated Task tab

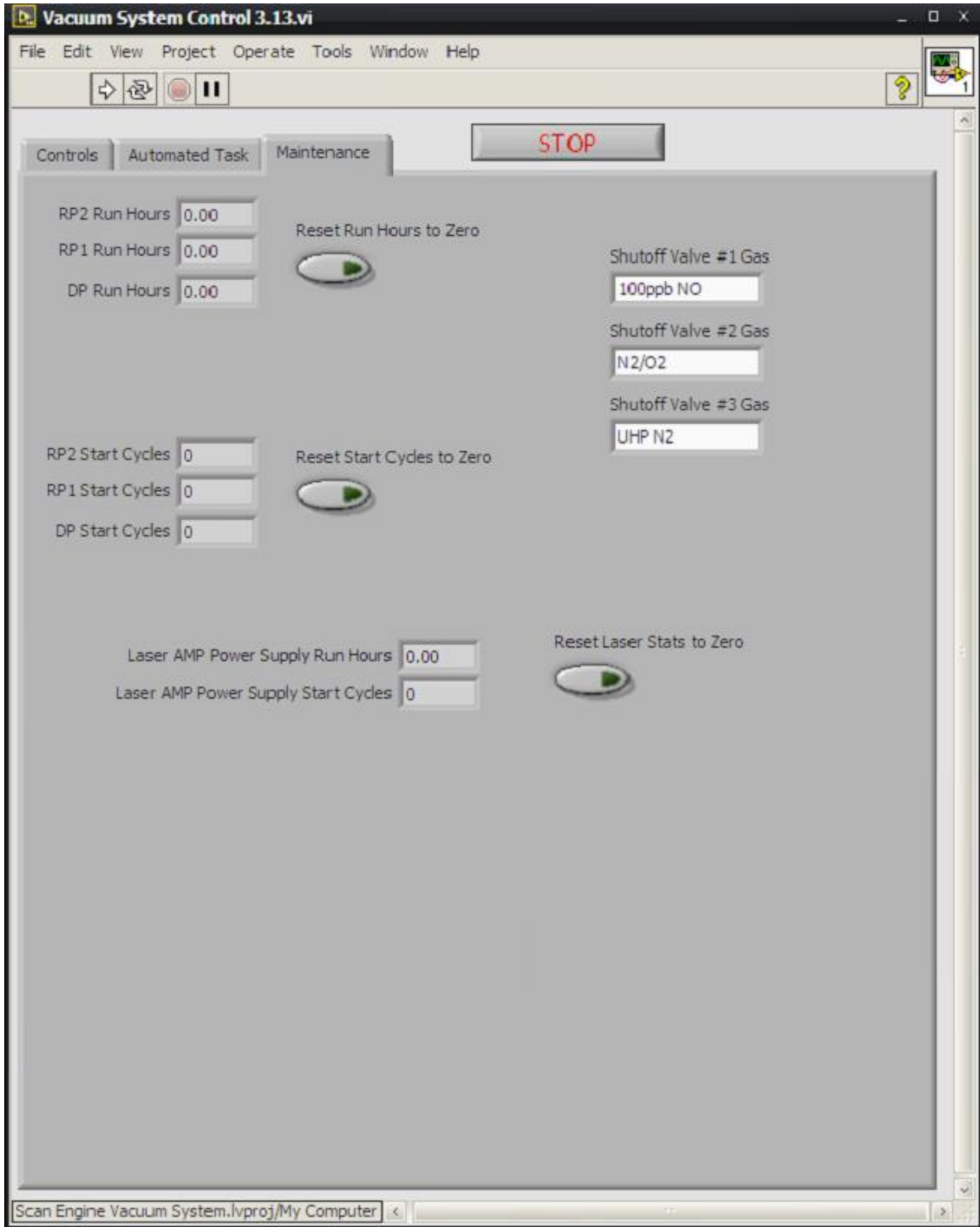


Figure 27. “Vacuum System Control.vi” Maintenance tab

“Ringdown Time.vi”

The *Ringdown Time* VI was highly modified from its previous version to accommodate the addition of the LIF system. The front panel features several useful indicators for the state of the vacuum system and two automated tasks for use with both LIF and CRDS experiments. Indicators and controls for each task are grouped together within the raised panels on the right side of the front panel. *Cycle Rad Cover* is used in conjunction with *Vacuum System Control.vi* to automate the opening and closing cycles of the radiation source cover. When used, it waits the duration of time specified in the *Tau0 Runtime* numeric field and then starts the *Rad Cover Cycle* task in *Vacuum System Control.vi*. The *Scan Dye Laser* task is used to step the dye laser through a specified wavelength range in the wavelength increment given. The task will stay at each wavelength until the number of data points specified have been collected. This task runs in conjunction with *Dye Laser Control.vi*. The *Setup Step Scan Ranges* button opens a dialog box to ask for the start and end wavelengths of the desired scan range and the number of times that range should be scanned. There are then two options: start the scan or specify an additional range. To remain at a single set wavelength for the duration of the data collection, the start and end wavelengths should be the same. The scan task will step the laser through each range in the order they were specified. The current range being scanned and its start and end wavelengths are displayed on the front panel. After the number of data points have been recorded, the LED of the *Setup Step Scan Ranges* button will turn off to indicate it has finished. It can also be turned off manually to abort the scans. The text file produced by the scan task is automatically labelled as the time stamp when the scan was started concatenated with “LIFexp.txt”.

The *Run State* panel displays the run state of the VI. The current run time since the start of the VI is shown at the top. This timer is reset each time a new scan is started. The *Write Data to File* button is used to record data for CRDS measurements, or can be used for LIF when a wavelength scan is not needed. File names for every data file are auto generated with the current time stamp followed by a label identifying the measurement system which collected the data. The program loops which calculate the ringdown and LIF data and statistics must be enabled using the labelled checkboxes. The comment box is used to add comments to the comment file generated for each dataset. This is useful when it is necessary to note problems or observations that occur during an experimental run. To save the comment to file, click the *Mark* button.

The statistics and graphs specific to the ringdown system are located on the *Ringdown* tab. The raw PMT signal vs time is shown at the top left. The decay constant is calculated from an exponential fit of the PMT signal. This value is added to the *Ringdown Time & Average Tau0* chart for each waveform collected to provide a graphical representation of its change over time. The *Run tau0 Average* button is used to calculate an average decay constant for a specified duration at the start of an experimental run. Once deselected, this value, τ_0 , is plotted on the *Ringdown Time & Average Tau0* chart along with the realtime value of the decay constant, τ , calculated from each fit. This gives a visual aid that quickly shows the deviation from the initial ringdown time as the experiment progresses. The parts-per-billion of the molecule being measured is displayed in the bottom chart. This is calculated using τ_0 , the realtime τ , cavity length, the speed of

light, and absorption cross-section for the molecule being measured. For more detail on this calculation, see the works of Reese and Gautrau.^{30, 31}

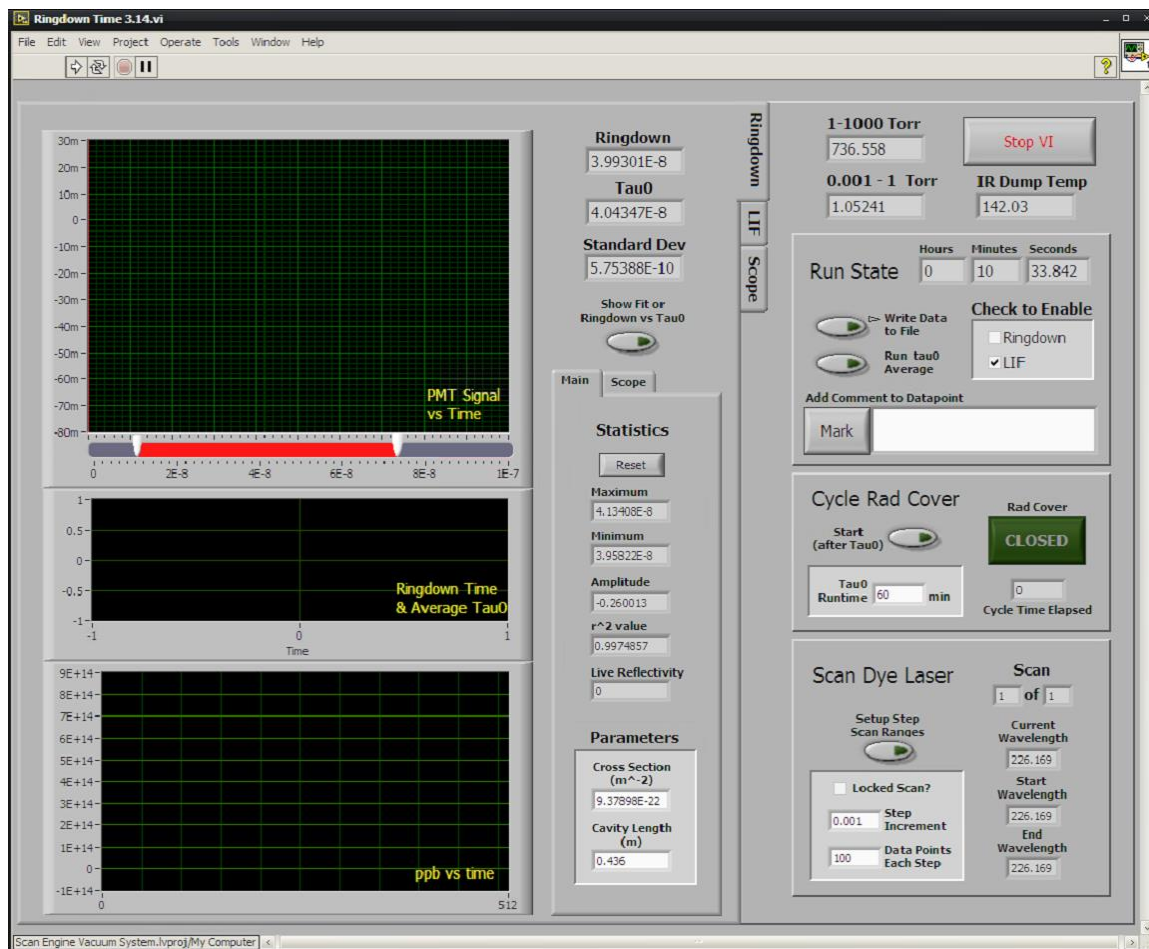


Figure 28. “Ringdown Time.vi” Ringdown tab

³⁰ Reese, “A System for Measuring Radiation Induced Chemical Products in Atmospheric Gases Using Optical Detection Methods.”

³¹ Gautrau, “Cavity Ringdown Spectroscopy in Nitrogen/Oxygen Mixtures in the Presence of Alpha Radiation.”

The *LIF* tab displays the fluorescence signal measured by the PMT scaled by the amplitude of the pulse measured by the photodiode. This helps to smooth pulse-to-pulse power fluctuations so that the series of measurements can be averaged. Below that chart is a chart that shows the raw signal measured by the photodiode. At the bottom is a chart that displays in realtime the fluorescence spectrum measured during a step scan. The x-axis is wavelength and the y-axis the average fluorescence at that wavelength. When using the Tektronix oscilloscope, the waveforms must be visible on the scope to be visible on this tab. The oscilloscope can be controlled from the VI using the *Scope* tab.

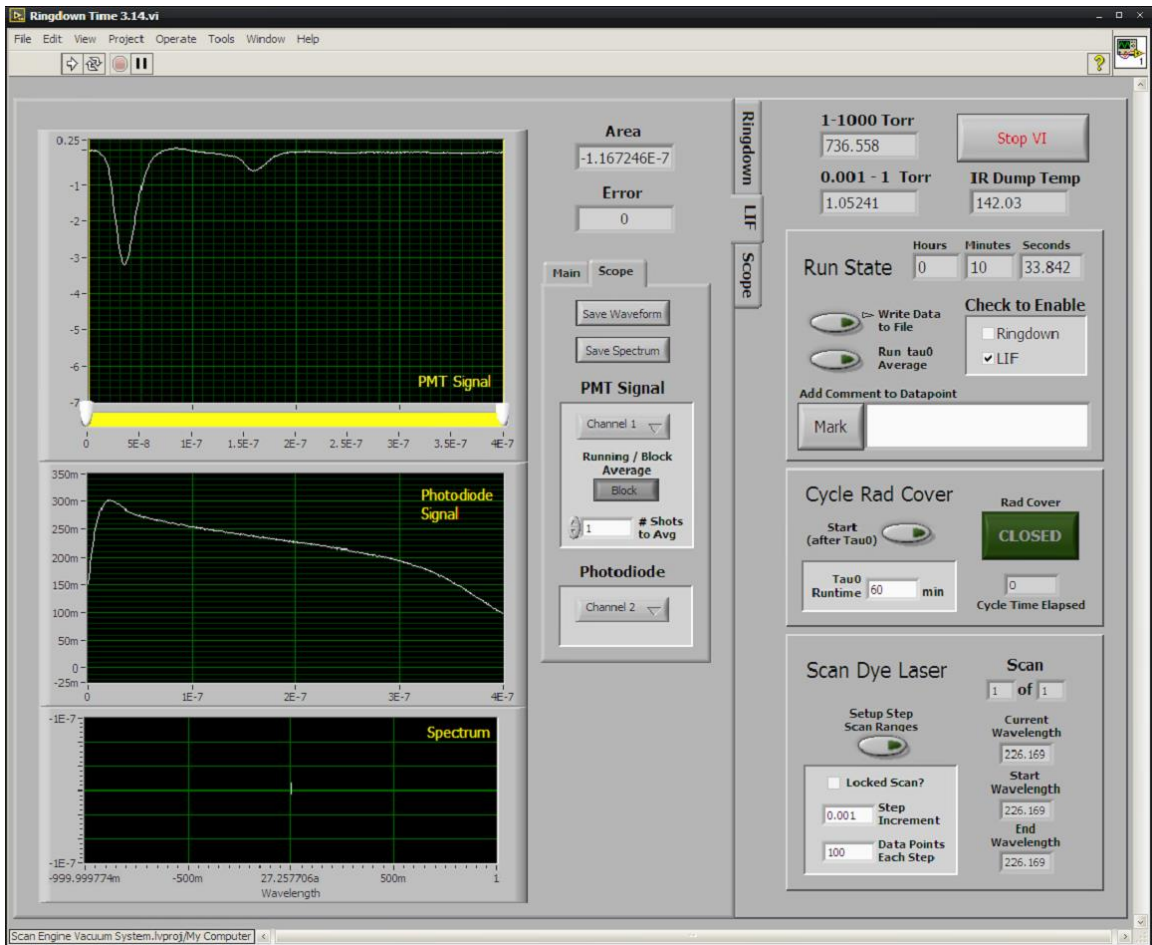


Figure 29. “Ringdown Time.vi” LIF tab

The *Scope* tab can be selected to operate either the PXI or the Tektronix oscilloscope. When using the oscilloscope, the waveforms must be fully visible on the scope screen to be visible here. Every setting available through the Tektronix LabVIEW drivers is available on this tab. At runtime, the VI will apply the settings defined here to the scope, but changes can be made directly from the scope once started; however, changing a single setting here will also reapply the values of the other settings, overwriting any changes made from the scope after VI startup. The drivers cannot access saved states on the oscilloscope. Saved states must be applied from the oscilloscope after VI start. Alternatively, if set from this tab, the value of each field can be saved as the default. Labels for each setting on this tab are identical to those of the oscilloscope and function as expected, except for vertical range. The range on the scope is specified as per major division. The range here must be specified as the total range on the scope screen, which consists of ten divisions.

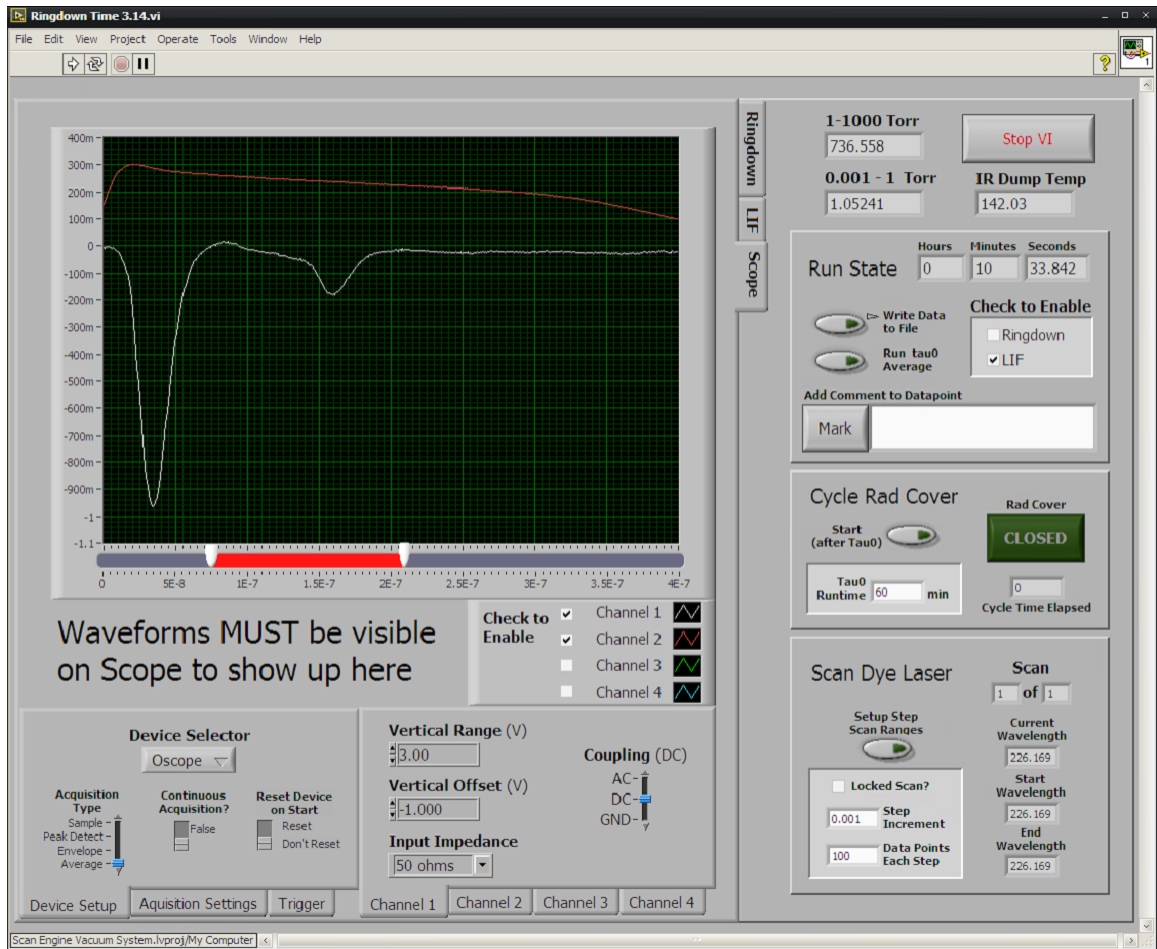


Figure 30. “Ringdown Time.vi” scope tab

“Dye Laser Control.vi”

The form and function of the dye laser control VI remains unchanged from its previous version except for the reassignment of the shared variables within its block diagram to refer to the shared variable library of the Windows XP computer to which it was transferred. Its front panel has been included to provide the reader with a visual

reference since it was mentioned many times in this paper. For a detailed description of its capability, see Gautrau's work.³²

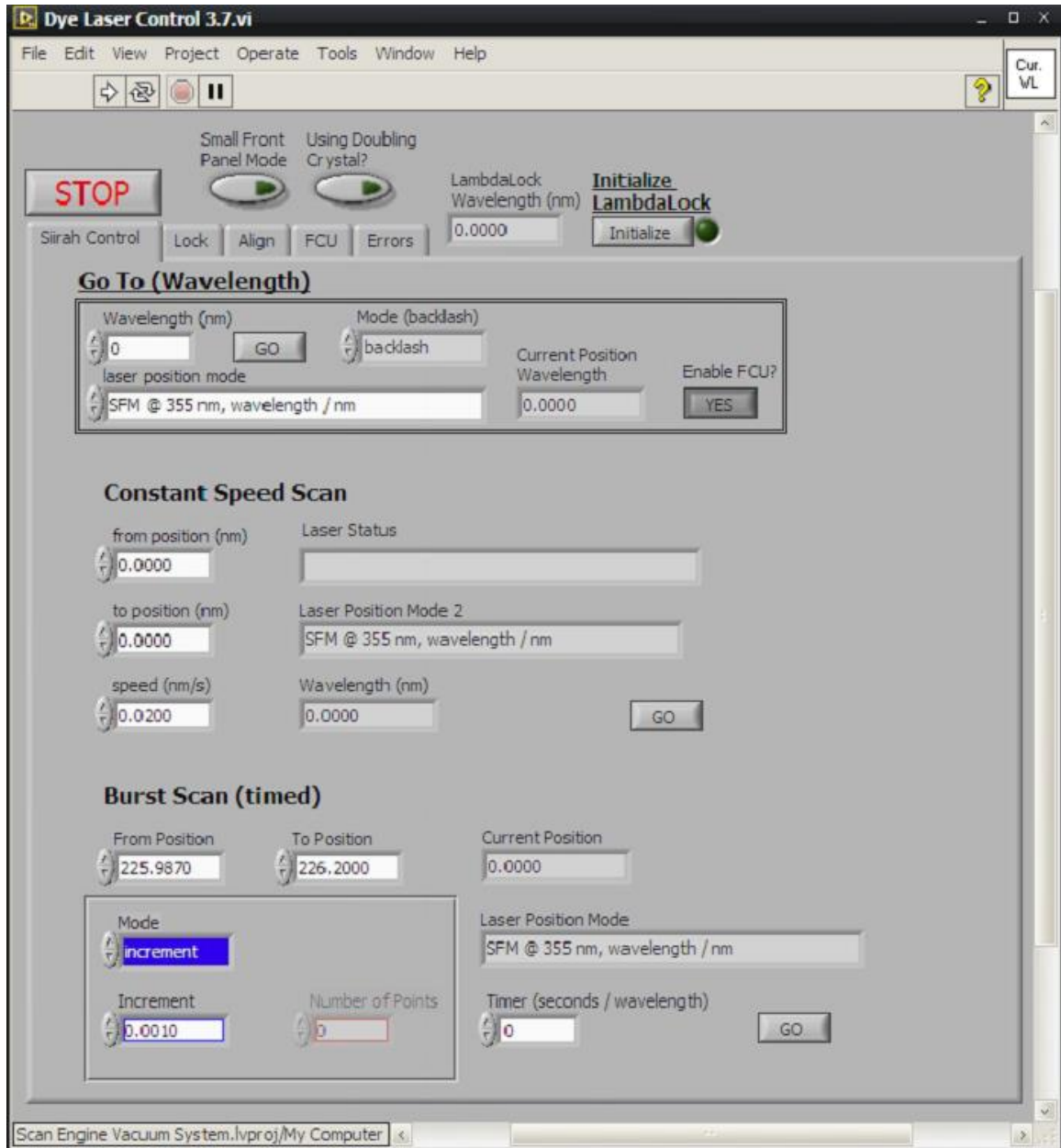


Figure 31. "Dye Laser Control" Sirah Control tab

³² Gautrau.

CHAPTER VII – SYSTEM VERIFICATION AND RESULTS

To verify the performance of the LIF system, a fluorescence signal needed to be collected while probing a gas mix for a molecule with a well-known fluorescence spectrum. Since the next task in the study of radiation-induced chemical products within the atmosphere is to measure the concentration of nitric oxide, NO was chosen for verifying the system and testing its sensitivity. NO fluoresces strongly when excited by wavelengths in the range of 225 nm to 227 nm. To cover this range, the FCU attached to the dye laser was modified to sum frequency mix 615 nm to 630 nm photons produced by a red dye with 355 nm photons produced by the Nd:YAG laser's third harmonic crystal as described in CHAPTER V. The Nd:YAG laser's second harmonic pumps DCM dye mixed in ethanol at 0.3 g/L as recommended by Sirah. This method produces a laser probe with a very narrow linewidth, high beam quality and long-lasting power. The oscilloscope collects and averages 32 waveforms and sends the averaged waveform to the computer. The computer integrates the PMT signal and scales the value by the maximum value recorded by the photodiode. This value is written to the text file and represents a single data point.

For the first verification runs, the LIF system was set to scan from 225.9 nm to 227.1 nm in steps of 0.005 nm. This range was chosen because it captures most of the prominent structure for NO fluorescence as determined by LIFBASE. LIFBASE is a Windows-based software program designed as a spectroscopy tool to chart the spectra of several diatomic molecules. It offers an absolute rovibrational emission and absorption

coefficients database and is available as freeware from SRI International.³³ SRI is an independent, nonprofit research center that works to bring advanced research and development from the laboratory to the marketplace. A screenshot showing a simulated emission spectrum for the $A^2\Sigma^+$ to $X^2\Pi$ transition is shown in Figure 32. $A^2\Sigma^+$ represents all possible vibrational bands and their rotational states for the first excited electronic state. Similarly, $X^2\Pi$ represents all vibrational bands and their rotational states within the electronic ground state.

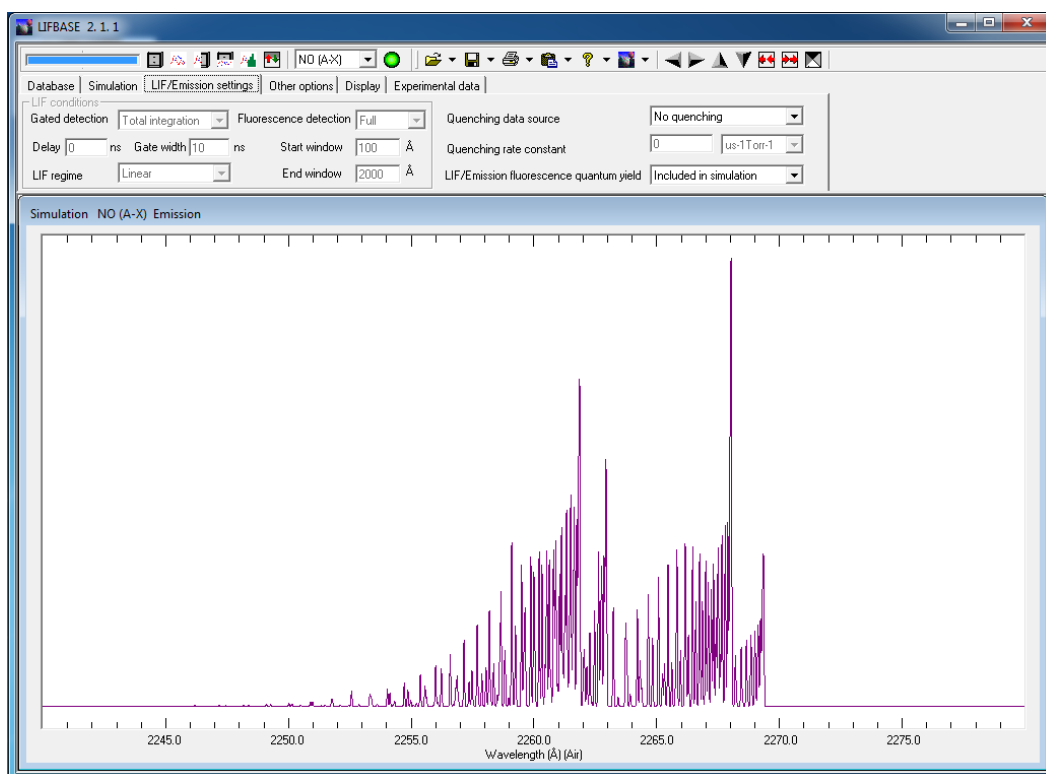


Figure 32. LIFBASE program and example spectrum

Screenshot of the LIFBASE program used to create the simulated excitation spectrum to compare with the spectrum collected experimentally to validate the LIF system.

³³ "LIFBASE Software Spectroscopy Tool | SRI International," accessed May 23, 2018, <https://www.sri.com/engage/products-solutions/lifbase>.

Remaining from a previous project, a certified mix of 5 ppm (\pm 250 ppb) NO₂ in a balance of N₂ was used for initial verification of the system. Absorption at these wavelengths causes NO₂ to photodissociate into a free oxygen atom and an NO molecule in an excited state. Because of this process, the fluorescence spectrum collected should be identical to that of NO. These runs helped to verify adequate linewidth resolution and determine system sensitivity so that a certified NO mix of an appropriate concentration could be ordered.

To flush the system of contaminants, the chamber was pumped down to \sim 75 mTorr and filled to \sim 740 Torr three times before being pumped down and filled with the NO₂ mix. The PMT was unfiltered and held to 1.06 kV between the first and last dynodes to amplify the fluorescence signal detected without overdriving the PMT. Ten scaled data points were collected at each step, averaged, and plotted against the input wavelength to produce a corrected excitation spectrum. A background spectrum was measured for UHP N₂ under the same conditions and subtracted from the NO₂ spectrum. The results are shown in Figure 33 along with the LIFBASE simulated spectrum scaled to fit.

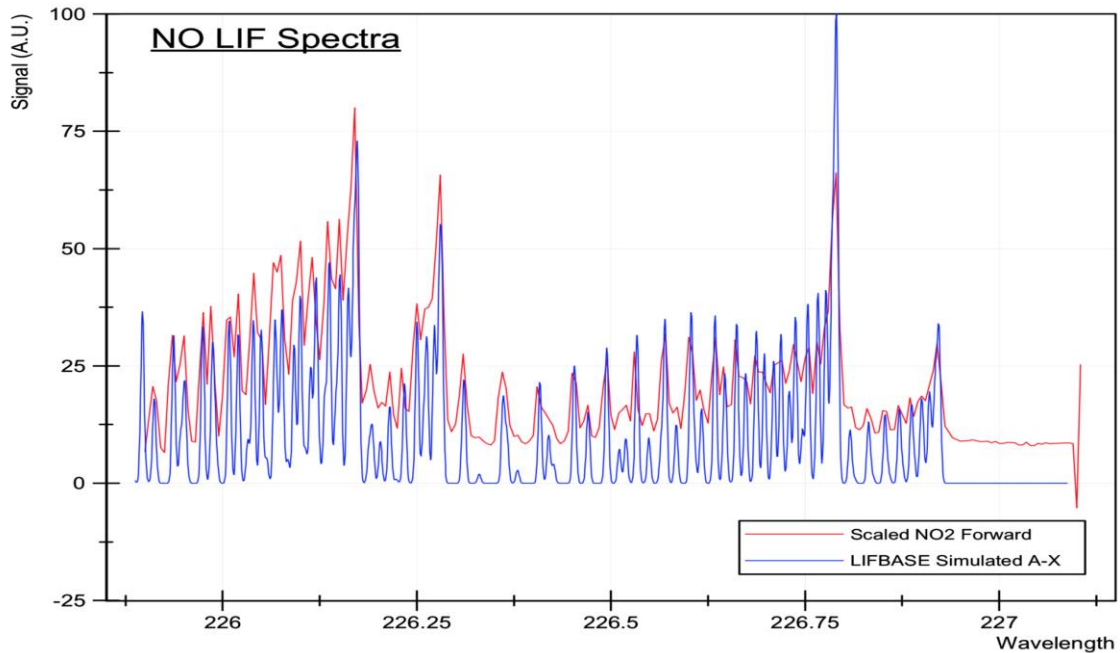


Figure 33. Spectrum from initial verification run with NO₂

Scaled/corrected excitation spectrum versus exciting wavelength (nm).

The results are consistent with those of the LIFBASE simulation. Although the LIFBASE simulation was also set to 0.005 nm steps, the effective linewidth of the laser is clearly sufficient to show the structure of the NO spectrum. To verify reproducibility and check for hysteresis, two runs were conducted stepping the exciting wavelength forward, from 225.9 nm to 227.1 nm, and two backward, from 227.1 nm to 225.9 nm, under the same conditions as before. The PMT was set to 1.06 kV. Three flush and fill cycles were done prior to filling with NO. Ten scaled data points were averaged for each step. The results are shown in the two plots associated with Figure 34 below.

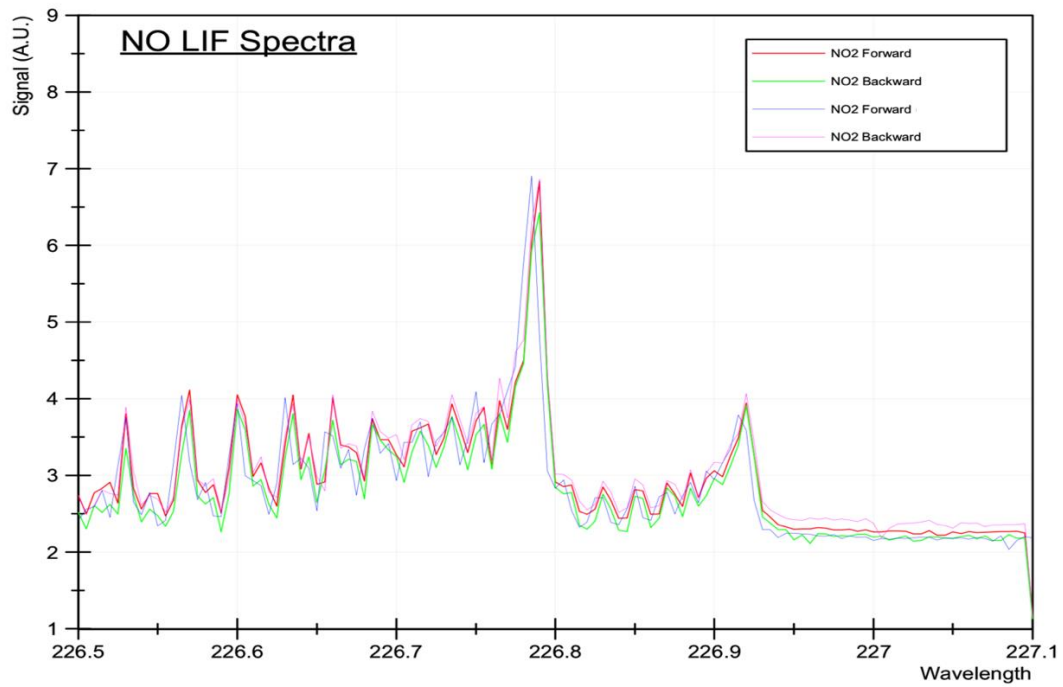
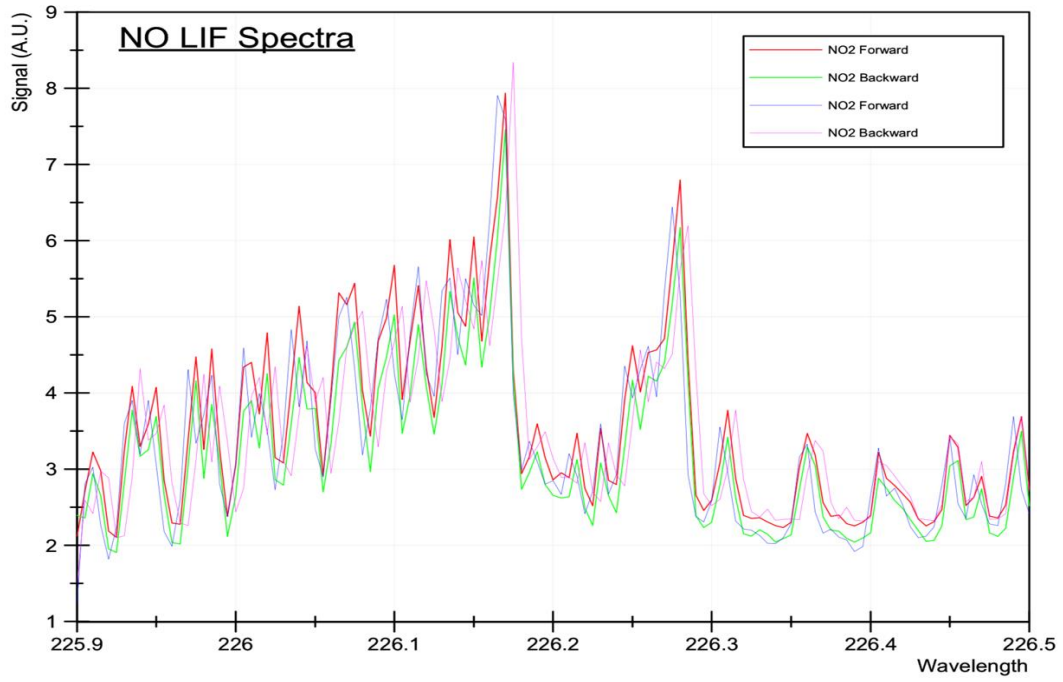


Figure 34. NO₂ Hysteresis and reproducibility check

Result of experimental trials to check for hysteresis. Excitation wavelength was stepped from 225.9 nm to 227.1 nm (Forward), then from 227.1 nm to 225.9 nm (Backward).

The plots show the signal response of the NO₂ mix to be consistent whether scanning forward or backward through the specified range of exciting wavelengths. Looking closely, the location of some peaks when stepping forward may be slightly offset from those when stepping backward; however, others appear to align well with one another suggesting the offset is likely due to the low number of averages used and not hysteresis. The amplitudes of each respective peak agree well across all runs supporting the validity of the method used for scaling each data point.

To determine system sensitivity to NO, several scans were conducted decreasing the effective concentration by 90% each successive run. Prior to the first run, the diffusion pump was used to bring the pressure down to $\sim 10^{-6}$ Torr during the three flush cycles. The gas introduction manifold was used to introduce a small, measurable volume of the NO₂ mix into the chamber until 7.4 Torr was reached. The chamber was then filled to ~ 740 Torr using UHP N₂. To compensate for any slight misalignment between the lens and PMT, a frosted glass optical filter was added to the PMT and the amplifier was adjusted to 1.13kV between the first and last dynodes for maximum amplification of the signal without overdriving. The scans were run from 225.9 nm to 227.1 nm in 0.005 nm steps. Ten data points were collected and averaged at each step. After each run, the chamber was pumped down to approximately 75 Torr and again filled with UHP N₂. Following the completion of these runs, an additional trial of low concentration was conducted under the same conditions for comparison with the previous. The diffusion pump was used during the three flush cycles. Using the volume of the gas introduction manifold, 250 mTorr of the NO₂ mix was added to the chamber before being filled to ~ 740 Torr with UHP N₂. The results of these data runs are shown in Figure 35.

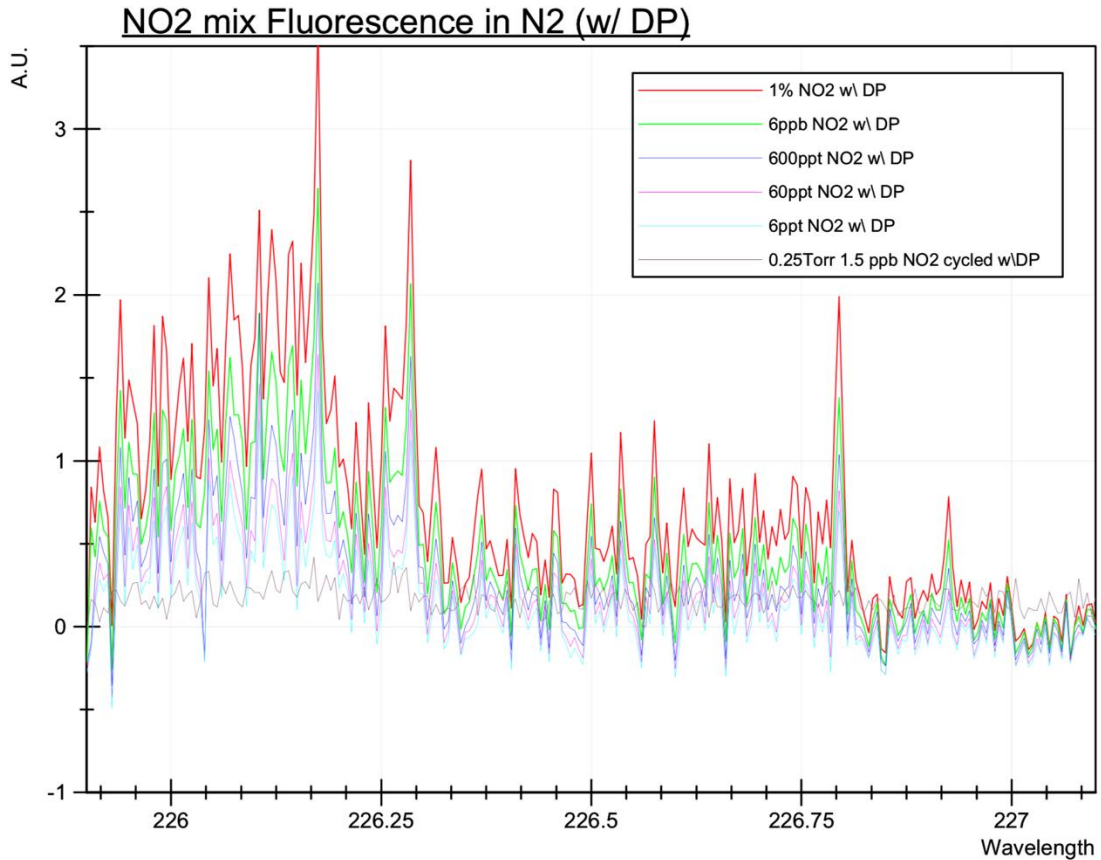


Figure 35. Fluorescence from NO₂ mix with decreasing concentration

Vertical axis: Fluorescence response in arbitrary units. Horizontal axis: Exciting wavelength in nm.

The results show a linear decrease in fluorescence signal that is proportional to the effective decrease in concentration. The structure of the NO excitation spectrum is distinguishable down to 6 ppt. The 0.25 Torr trial does not agree with the concentration approximated from the successively reduced trials, although the NO structure appears to be visible when compared with the other trials. Further investigation is required to discover the reason for this discrepancy, but the results did help to select an appropriate concentration of NO mix to purchase. Since Cantera predicts the concentration of NO in radiated air mixtures to be around 400 ppb and the fluorescence appears to be measurable

in that range by either method of dilution, a certified mix of 100 ppb (± 50 ppb) NO in a balance of N₂ was obtained.

The certified NO mix was used to test the sensitivity of the LIF system to NO in exactly the same way as it was done using the NO₂ mix. The diffusion pump was used to flush the chamber three times before it was filled to ~740 Torr with the certified NO mix. The experimental configuration and PMT settings remained unchanged from the previously described experimental trials. Ten data points were collected and averaged at each step. A full spectrum was collected at 100% of the concentration mentioned in 0.005 nm step increments. For comparison, a second data set was collected at full concentration from 226.16 nm to 226.22 nm with a step increment of 0.001 nm to determine whether the added resolution translated to higher peaks at more precisely specified wavelengths. After the short run at full concentration, the vacuum chamber was pumped down to ~370 Torr and backfilled to ~740 Torr with UHP N₂. The scan range was limited to the area around the major peaks near 226.2 and 226.8 nm and the step increment was set to 0.0025 nm to speed up data collection. Datasets were collected reducing the effective concentration by 50% each time until reaching 1.5% of the full concentration; this correlates to an approximate NO concentration of 2 ± 0.8 ppb. A full spectrum was recorded for the final run at 1.5% for comparison with the one collected at 100%. The raw data collected during these runs are shown in Figure 36. It was clear after viewing the raw datasets that the smaller steps produced more prominent peaks which could possibly yield better spectra. Subtracting the 1.56% dataset from the others would produce very similar results. For this reason and in the interest of time, no N₂ baseline dataset was collected to process the data further.

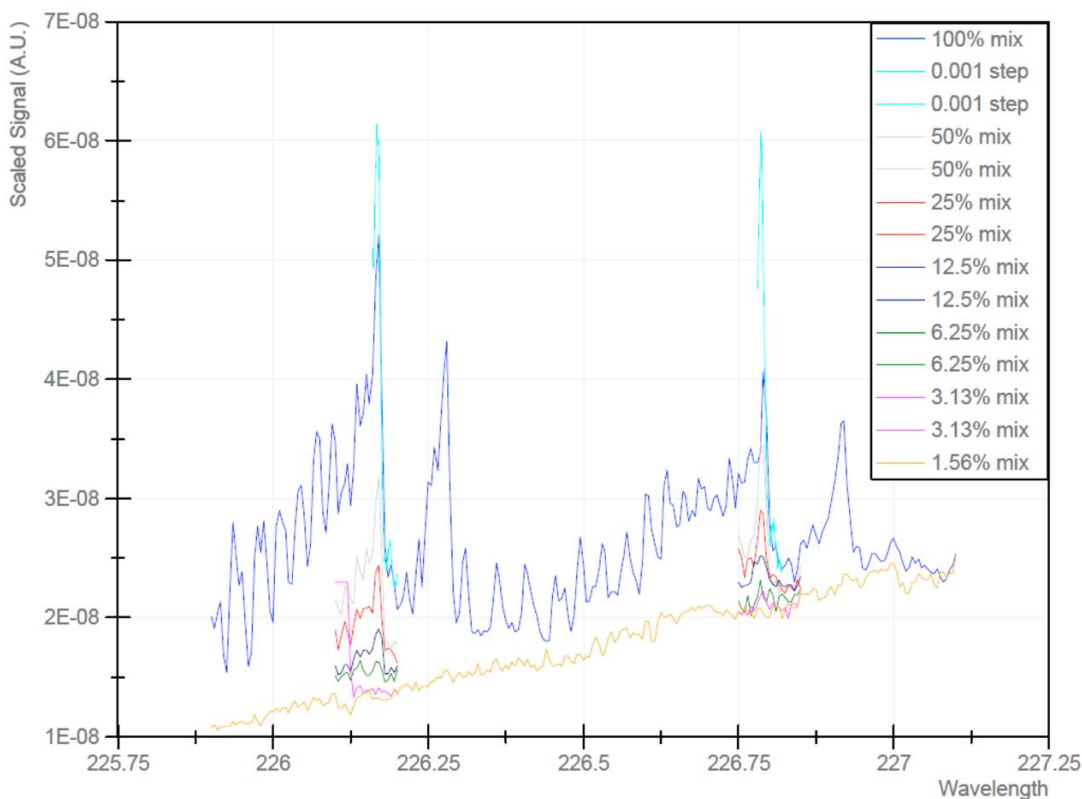


Figure 36. Raw fluorescence signal with decreasing concentration

Vertical Axis: Scaled fluorescence response in arbitrary units. Horizontal axis: Exciting wavelength in nm.

The amplitude of the scaled signal appears to decrease by 50% with each corresponding decrease in concentration, indicating a proportional relationship consistent with those collected from the certified NO₂ mix. The separation between the spectra near the peak around 226.2 nm is much greater than the one around 226.8 nm which suggests this peak is more appropriate for detecting low NO concentrations in a background of N₂. For this reason, a second set of data was collected using higher resolution over a narrow band around this peak. A full spectrum was recorded for N₂ after three flush cycles using 0.005 nm steps for speed under the same conditions as before. After this, an additional full spectrum was recorded for the full concentration of the NO mix. For each successive

run after this, the chamber was pumped down to ~370 Torr before being backfilled with UHP N₂ until ~740 Torr is reached, again effectively reducing concentration by half. The exciting wavelength was scanned from 226.16 nm to 226.18 nm under the same conditions used prior except in 0.001 nm steps. This procedure was stopped once reaching a concentration of 0.78% of the full mix, or 0.8 ± 0.4 ppb. The values recorded for the N₂ scan were then subtracted from those of the NO scans. The results are shown in Figure 37 which helps show the proportionality between each spectrum. Because of the large difference in scale, Figure 38 shows the processed datasets starting at 25% concentration of the full mix.

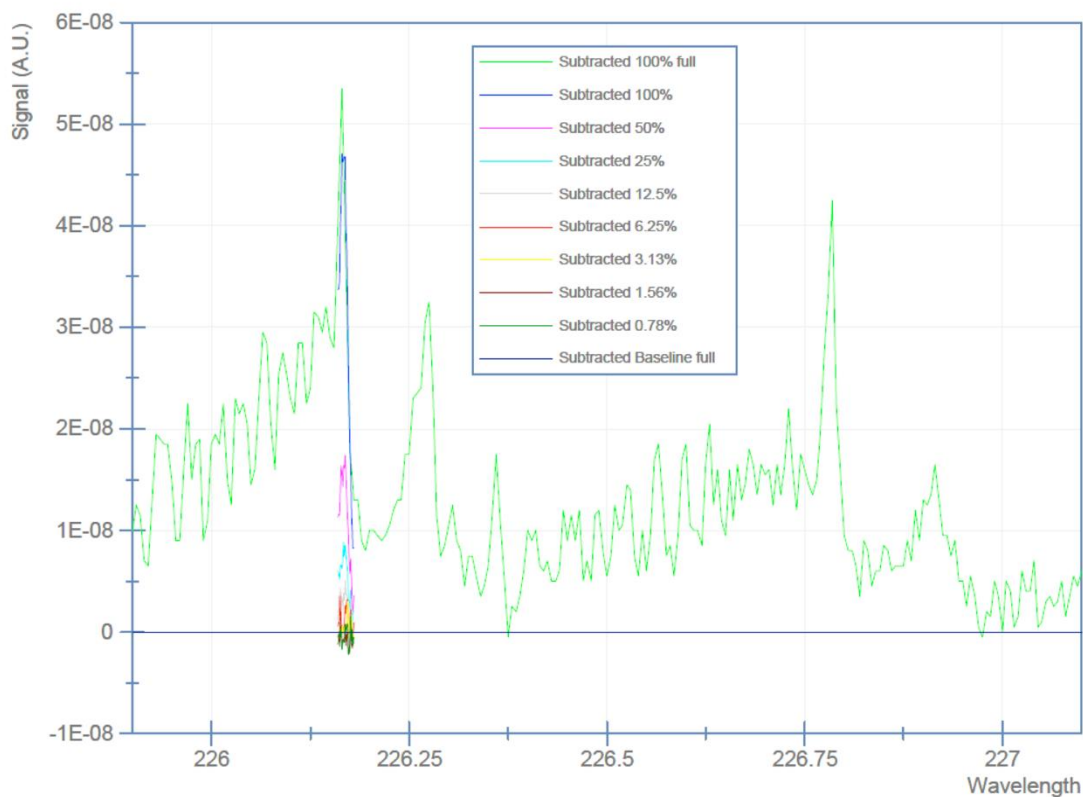


Figure 37. NO fluorescence response with decreasing concentration

0.005 nm steps were used for the full runs from 225.9 nm to 227.1 nm. 0.001 nm steps were used for the short range runs between 226.16 nm and 226.18 nm

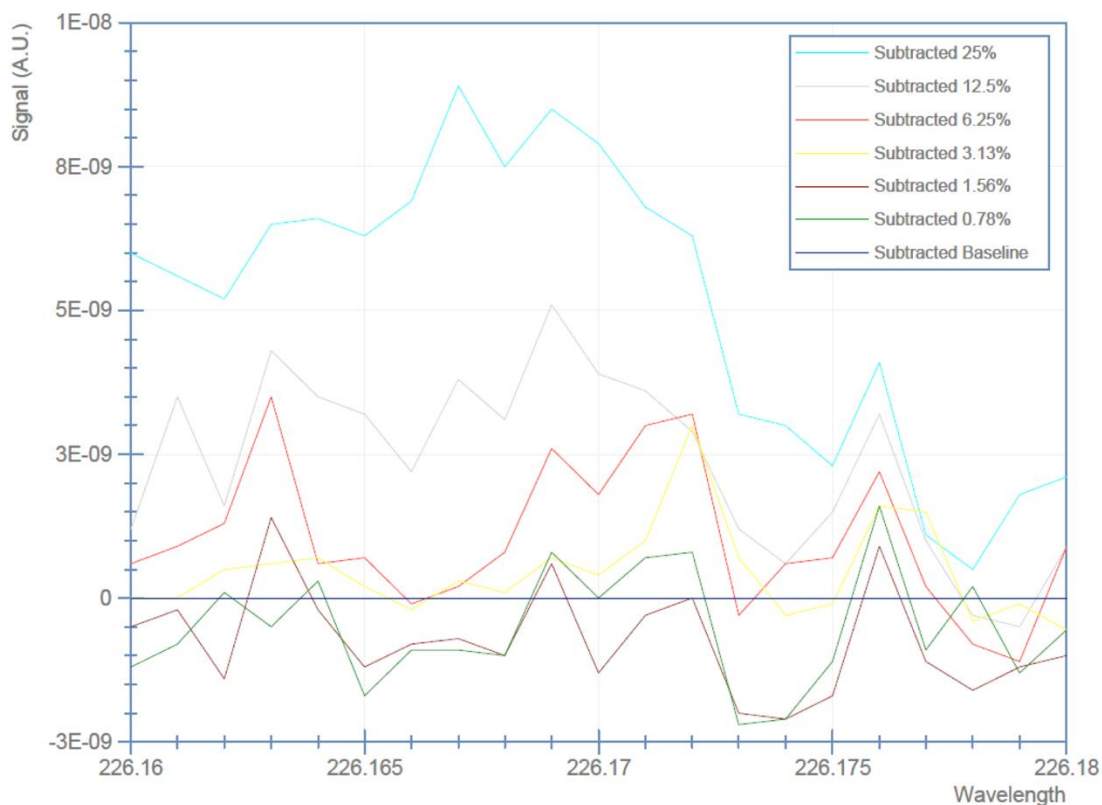


Figure 38. NO fluorescence response from lowest concentrations

Lowest concentrations from Figure 37 shows excitation spectrum from 226.16 nm to 226.18 nm in steps of 0.001 nm.

While the maximum amplitude for the two highest concentrations is at 226.167 nm, the low concentrations plot shows the peak is not as prominent for low concentrations. The minor peak at 226.171 nm appears to have the greatest correlation with each reduction in concentration but lacks the separation the stronger peaks have. The amplitude at 226.169 nm is strong at both the high and low concentrations and provides a large separation between each. The spectra of Figure 38 were integrated in an effort to improve the detection limit for this configuration. Figure 39 shows the integrated spectra.

Assuming only the positive curves indicate a detected signal, the current system configuration has a detection limit in the range of 3 ± 2 ppb in an N_2 background.

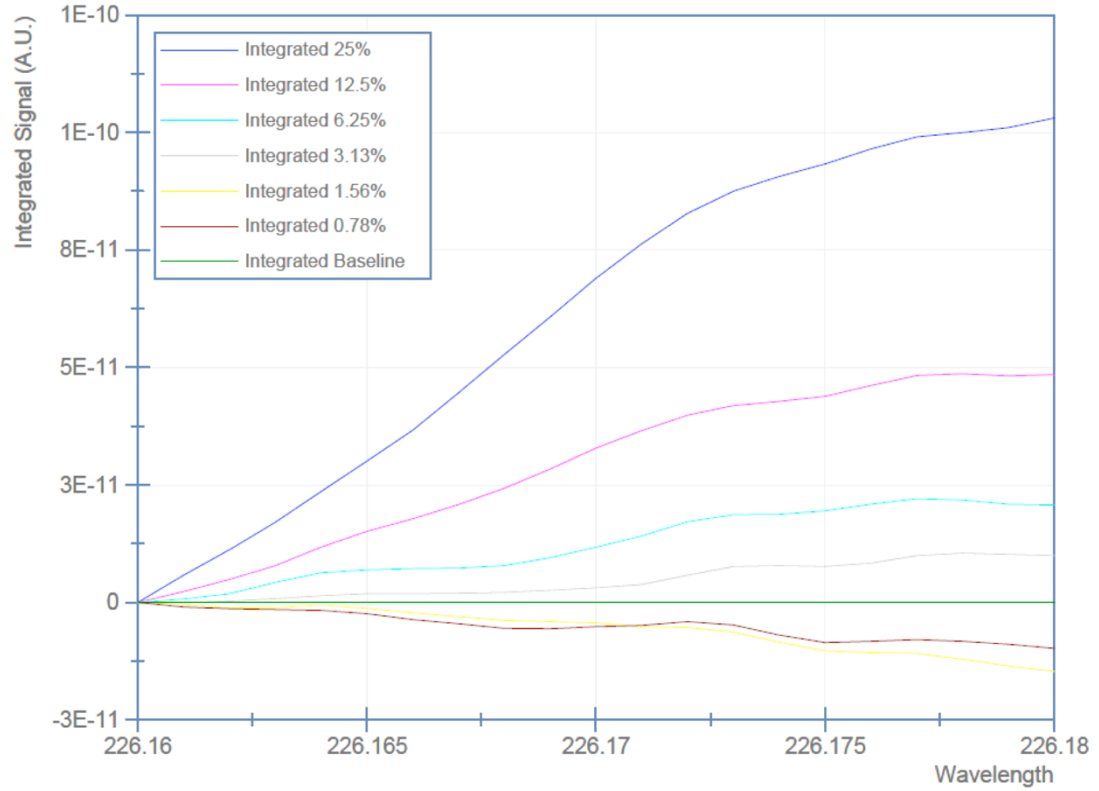


Figure 39. Integrated NO fluorescence response

Integrated excitation spectrum from Figure 38 used to experimentally approximate a minimum detection limit.

CHAPTER VIII – CONCLUSIONS AND FUTURE WORK

The results presented in the preceding section indicate, with the current configuration, the LIF system is capable of detecting NO at concentrations of 3 ± 2 ppb in a background of N₂. The final procedure should be repeated to test the validity of these observations, but 226.169 nm may serve as the best exciting wavelength for probing mixtures for NO. Further refinements such as adjustments to the PMT voltage, improvements to the DAQ system, and the use of software filters will no doubt improve reproducibility and system sensitivity.

The completion and verification of the LIF system opens the door to numerous fluorescence experiments related to the validation of the computation model being developed. As previously stated, radiation-induced NO will be the first molecule to be probed in a dry N₂/O₂ 80/20 mix. If a quantifiable measurement can be made, production rates will be compared with those of ozone to refine the present model. NO₃ is believed to be the eventual result from the time evolution of NO and NO₂. It is known to fluoresce at ~623 nm which would only require changing the turning mirrors that direct the exciting beam to the chamber. If NO and NO₂ are found in the irradiated dry air mix, HNO₂ is to be suspected with the addition of water vapor. HNO₂ has a strong absorption cross section at ~355 nm. A set of ringdown mirrors are on hand to make CRDS measurements using the Nd:YAG laser's third harmonic once the NO investigation is complete.

A typical quantitative calculation from an LIF signal is based on the geometry between system components which introduces significant error. It is clear from the results that the fluorescence response increases proportionally with concentration. Although only

valid for a specific configuration, the certified NO mix can be used to calibrate the LIF system by mapping the fluorescence response to increasingly diluted concentrations and calculating a fit. While sufficient to verify the functionality of the LIF system, using UHP N₂ as the diluting gas to map the fluorescence response to an effective NO concentration may not be appropriate for experiments with the goal of detecting NO induced by alpha radiation in the atmosphere. These experiments will have a background mixture of 80% N₂ and 20% O₂. Fluorescence response and system sensitivity may be substantially different with the addition of O₂. It will be necessary to use an N₂/O₂ mixture to dilute the NO mix so that the results can be compared with those recorded while using UHP N₂.

The Tektronix 3054B oscilloscope was chosen for data acquisition because of its high sample rate of 5 GS/s. The 10BASE-T Ethernet port used to transmit the averaged waveform to the computer only has a transfer speed of 10 Mb/s. Only one waveform can be transferred at a time. Since the current system configuration uses two channels, the second waveform must be saved to the oscilloscope's internal memory while the first is being sent. Each waveform is sent with a waveform preamble indicating horizontal and vertical scales and other settings in place when the waveform was created. There are 500 14-bit data points in each waveform. Because of all this, the number of waveforms that can be sent to the computer have been observed to be approximately four per second when in single acquisition mode, and one every 1.6 seconds when sending an averaged waveform.

A possible remedy to this problem would be to purchase a communications card for the oscilloscope which adds a GPIB interface. Although GPIB has approximately the same listed bit-rate as 10BASE-T Ethernet, it is a parallel bus and provides many

advantages over Ethernet in this specific case. The Tektronix programmers' manual has 330 pages of commands to control many nuance settings through the GPIB interface that decrease transfer times which is not possible through the 10BASE-T Ethernet port. An alternative method to effectively increase transfer rates is to use the PXI to record the signal from the photodiode so that the oscilloscope need only transfer a single waveform each time. This would also reduce the internal processing time the oscilloscope requires to store the second waveform in its local memory and recall it for sending after the first is transferred. The latter would require less time to implement and has the potential to be more effective since transfer times would be essentially cut in half.

APPENDIX A – Permission Emails

Thursday, June 21, 2018 at 3:22:12 PM Central Daylight Time

Subject: FW: Customer Contact
Date: Thursday, June 21, 2018 at 1:58:17 PM Central Daylight Time
From: Oliver, Kevin
To: Patrick Ables

Dear Patrick,

Your below email request was forwarded to me. Please accept this email as permission for your request. PerkinElmer requests that, if possible, you please print under Figure the following text: "© 2010-2018 PerkinElmer, Inc. All rights reserved. Printed with permission."

Thank you.

Best regards,

Kevin A. Oliver | Vice President and Chief Intellectual Property Counsel
[PerkinElmer | For the Better](#)
kevin.oliver@perkinelmer.com
Phone: +1 781.663.5786 | Fax: +1 781.663.5968
940 Winter Street, Waltham, MA 02451 USA
www.perkinelmer.com

Please consider the environment before printing this e-mail.
This e-mail message and any attachments are confidential and proprietary to PerkinElmer, Inc. If you are not the intended recipient of this message, please inform the sender by replying to this email or sending a message to the sender and destroy the message and any attachments. Thank you.

Comments/Questions

Hello, I am a student writing a master's thesis at the University of Southern Mississippi in the United States. I would like to ask for your permission to use a figure from a manual in which you have the copyright: "An Introduction to Fluorescence Spectroscopy" The figure is on page 7 and titled Figure 1: Transitions giving rise to absorption and fluorescence emission spectra. If you grant me permission, this email and your response will be included in an appendix in the master's thesis. The title will be A SYSTEM FOR CONDUCTING LASER-INDUCED FLUORESCENCE MEASUREMENTS ON GAS MIXTURES EXPOSED TO ALPHA RADIATION. If you have any questions, please contact me at patrick.ables@usm.edu Thanks you, Patrick Ables

Contact Information

First Name:

Page 1 of 3

Thursday, June 21, 2018 at 3:20:16 PM Central Daylight Time

Subject: RE: Permission to use a figure from your paper
Date: Wednesday, June 20, 2018 at 8:22:01 AM Central Daylight Time
From: Wynn, Charles - 0991 - MITLL
To: Patrick Ables

Patrick,

You have permission to use the figure. Good luck!

Chuck

Charles M. Wynn, Ph.D.
MIT Lincoln Laboratory
244 Wood Street
Lexington, MA 02420-9108
Phone: (781) 981-3132
Fax: (781) 981-4983
<https://www.ll.mit.edu/mission/electronics/cmnt/bios/wynn-c.html>

From: Patrick Ables <Patrick.Ables@usm.edu>
Sent: Tuesday, June 19, 2018 6:31 PM
To: Wynn, Charles - 0991 - MITLL <cwynn@ll.mit.edu>
Subject: Permission to use a figure from your paper

Hello, I am a student writing a master's thesis at the University of Southern Mississippi. I would like to ask for your permission to use a figure from a paper you co-authored:

"Noncontact Detection of Homemade Explosive Constituents via Photodissociation Followed by Laser-Induced Fluorescence."

The figure is attached to this email and depicts the transitions between energy levels for specific exciting wavelengths and the fluorescence emission that follows.

If you grant me permission, this email and your response will be included in an appendix in the master's thesis. The title will be A SYSTEM FOR CONDUCTING LASER-INDUCED FLUORESCENCE MEASUREMENTS ON GAS MIXTURES EXPOSED TO ALPHA RADIATION.

If you have any questions, please contact me at patrick.ables@usm.edu

Thanks you,
Patrick Ables

Page 1 of 1

Thursday, June 21, 2018 at 3:21:03 PM Central Daylight Time

Subject: Re: Request for permission
Date: Tuesday, June 19, 2018 at 6:55:08 PM Central Daylight Time
From: Sidney Gautrau
To: Patrick Ables

You have my permission.
Sidney

From: Patrick Ables <Patrick.Ables@usm.edu>
Date: Tuesday, June 19, 2018 at 6:28 PM
To: Sidney Gautrau <Sidney.Gautrau@usm.edu>
Subject: Request for permission

Hello Sidney,

I would like to ask your permission to use several photos you used in your master's thesis titled: CAVITY RINGDOWN SPECTROSCOPY IN NITROGEN/OXYGEN MIXTURES IN THE PRESENCE OF ALPHA RADIATION. I have attached a screenshot of all the photos and listed the respective figure titles from your thesis below. I would like to reproduce these images to show the initial state of the vacuum system prior to my modifications.

If you grant me permission, this email and the reply will be included in an appendix in the master's thesis. The title will be A SYSTEM FOR CONDUCTING LASER-INDUCED FLUORESCENCE MEASUREMENTS ON GAS MIXTURES EXPOSED TO ALPHA RADIATION.

If you have any questions please contact me at patrick.ables@usm.edu

Thanks you,
Patrick Ables

Figures:

Figure 6. Aluminum source holder and radiation source cover.

Figure 9. Previously modified 8" flange for CRD cavity.

Figure 11. PXI used for data acquisition.

Figure 12. Dye Laser and Nd:YAG laser.

Figure 14. UGA table with adjustable height.

Figure 17. PMT used in 266nm configuration.

Page 1 of 1

Friday, June 22, 2018 at 12:41:44 PM Central Daylight Time

Subject: Re: Request for permission
Date: Friday, June 22, 2018 at 12:37:05 PM Central Daylight Time
From: Tyler Reese
To: Patrick Ables

Patrick,

Yes, you most certainly have my permission to reproduce the table you have indicated in your email.

-Tyler Reese

From: Patrick Ables
Sent: Tuesday, June 19, 2018 6:57:17 PM
To: Tyler Reese
Subject: Request for permission

Hello Tyler,
I would like to ask your permission to reproduce a table you created from data used for your master's thesis titled: "*A System for Measuring Radiation Induced Chemical Products in Atmospheric Gases Using Optical Detection Methods.*"

I have attached a screenshot of the table your thesis referenced as Table 2.1 *Penetration Depth Comparison for Representative Radiation Sources*

If you grant me permission, this email and the reply will be included in an appendix in the master's thesis. The title will be A SYSTEM FOR CONDUCTING LASER-INDUCED FLUORESCENCE MEASUREMENTS ON GAS MIXTURES EXPOSED TO ALPHA RADIATION.

If you have any questions please contact me at patrick.ables@usm.edu

Thanks you,
Patrick Ables

Page 1 of 1

APPENDIX B

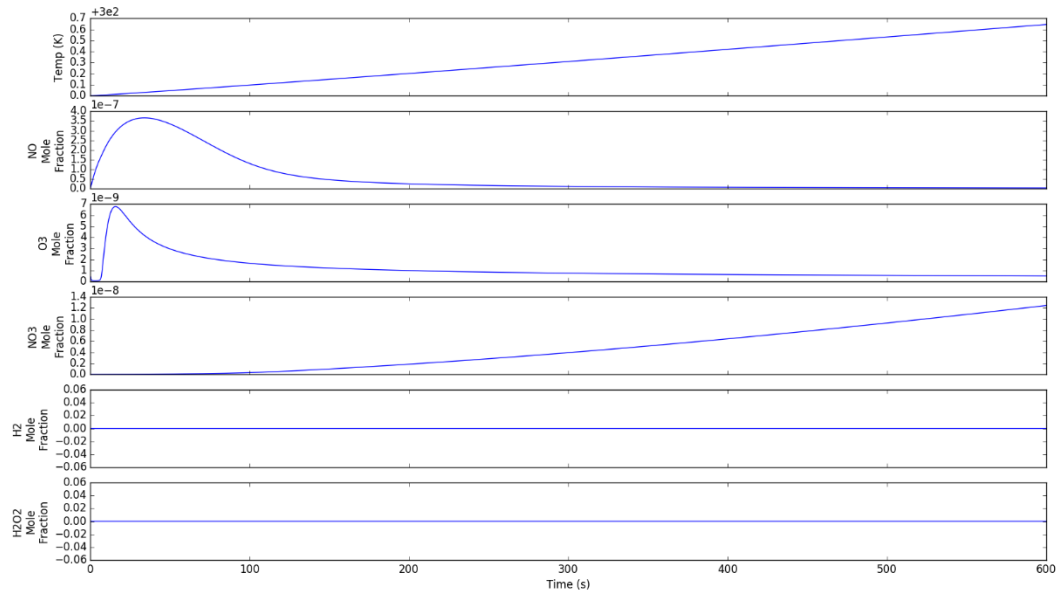


Figure A1. Cantera Model 0% RH with all electrons

Cantera calculated molar fraction for nitric oxide, ozone, and NO_3 . (SOURCE: Winstead 2017)

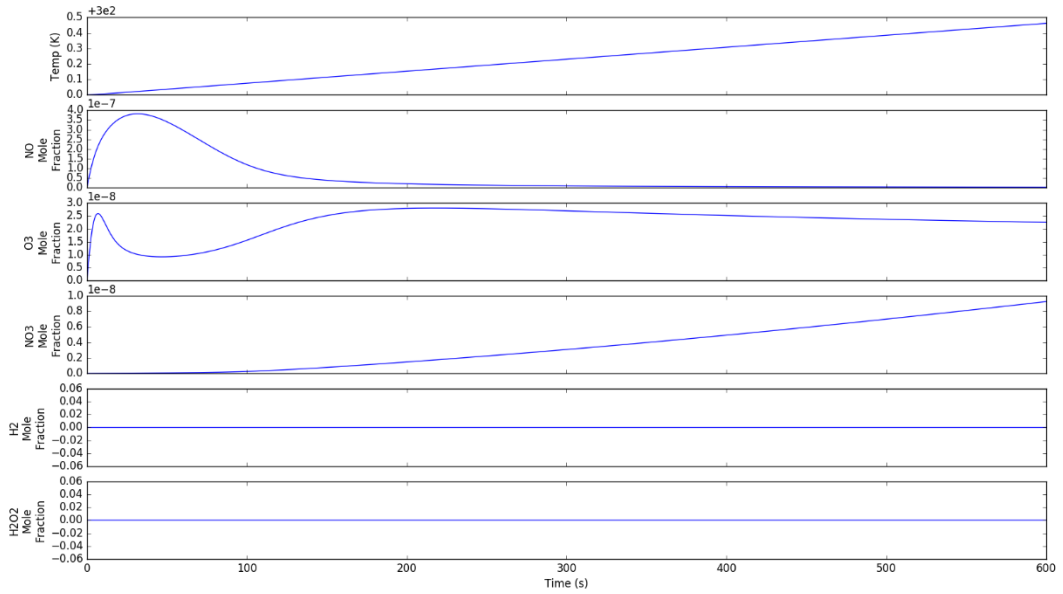


Figure A2. Cantera Model 0% RH with 1% electrons

(SOURCE: Winstead 2017)

REFERENCES

- Buchanan, Aubri Capri. *Characterization of Air Fluorescence Induced by Alpha Radiation*. University of Southern Mississippi, 2008.
- Christensen, Doran M., Carol J. Iddins, and Stephen L. Sugarman. "Ionizing Radiation Injuries and Illnesses." *Emergency Medicine Clinics of North America* 32, no. 1 (February 2014): 245–65. <https://doi.org/10.1016/j.emc.2013.10.002>.
- Crosley, David R. "Laser-Induced Fluorescence in Spectroscopy, Dynamics, and Diagnostics." *Journal of Chemical Education* 59, no. 6 (June 1982): 446. <https://doi.org/10.1021/ed059p446>.
- Gautrau, Sidney. "Cavity Ringdown Spectroscopy in Nitrogen/Oxygen Mixtures in the Presence of Alpha Radiation," 2016. https://aquila.usm.edu/masters_theses/258.
- L'Annunziata, Michael F. *Radioactivity: Introduction and History*. Elsevier, 2007.
- "LIFBASE Software Spectroscopy Tool | SRI International." Accessed May 23, 2018. <https://www.sri.com/engage/products-solutions/lifbase>.
- Mcfadyen, Aubrey D. "Samuel C. Lind." *Chemical & Engineering News* 25, no. 23 (June 9, 1947): 1664. <https://doi.org/10.1021/cen-v025n023.p1664>.
- Miller, Dudley G. *Radioactivity and Radiation Detection*. Gordon and Breach Science Publishers, 1972.
- "Palos Verdes Radon." United States Geological Survey. Accessed December 24, 2017. <https://pubs.usgs.gov/of/2004/1050/PalosVerdesRn.htm#uranium.htm>.
- Paschotta, Rudiger. "Frequency Doubling." *Encyclopedia of Laser Physics and Technology*. Accessed May 19, 2018. https://www.rp-photonics.com/frequency_doubling.html.

- Price, William James. *Nuclear Radiation Detection*. McGraw-Hill, 1964.
- Reese, Tyler. "A System for Measuring Radiation Induced Chemical Products in Atmospheric Gases Using Optical Detection Methods." Master's Thesis, The University of Southern Mississippi, 2010.
- Turner, J. E. *Atoms, Radiation, and Radiation Protection*. 3rd completely rev. and enl. ed. Physics Textbook. Weinheim: Wiley-VCH, 2007.
- <http://nuclear.dababneh.com/Radiation-Undergrad/Atoms, Radiation, and Radiation Protection.pdf>.
- Williams, A.T.R. *An Introduction to Fluorescence Spectroscopy*. Perkin-Elmer, 1981.
- <https://books.google.com/books?id=CVL-ewEACAAJ>.
- Winstead, Chris. "2017 Annual Report DTRA." The University of Southern Mississippi, 2017.
- Wynn, C. M., S. Palmacci, R. R. Kunz, and M. Rothschild. "Noncontact Detection of Homemade Explosive Constituents via Photodissociation Followed by Laser-Induced Fluorescence." *Optics Express* 18, no. 6 (March 15, 2010): 5399.
- <https://doi.org/10.1364/OE.18.005399>.